Accelerating gene discovery by phenotyping whole-genome sequenced multi-mutation strains and using the sequence kernel association test (SKAT)

Tiffany A. Timbers[1], Stephanie J. Garland[2], Swetha Mohan[1], Stephane Flibotte[2], Mark Edgley[2], Quintin Muncaster[1], Vinci Au[2], Erica Li-Leger[2], Federico I. Rosell[3], Jerry Cai[1], Suzanne Rademakers[4], Gert Jansen[4], Donald G. Moerman[2] and Michel R. Leroux[1]*

[1]Department of Molecular Biology and Biochemistry and Centre for Cell Biology, Development, and Disease, Simon Fraser University, 8888 University Drive, Burnaby, British Columbia, V5A 1S6 Canada

[2]Department of Zoology, University of British Columbia, 2350 Health Science Mall, Vancouver, British Columbia, V6T 1Z3 Canada

[3]Department of Biochemistry and Molecular Biology, University of British Columbia, 2350 Health Science Mall, Vancouver, British Columbia, V6T 1Z3 Canada

[4]Department of Cell Biology, Erasmus MC, PO Box 2040, 3000 CA, Rotterdam, The Netherlands

*Corresponding author

Email: leroux@sfu.ca

Abstract

Forward genetic screens represent powerful, unbiased approaches to uncover novel components in any biological process. Such screens suffer from a major bottleneck, however, namely the cloning of corresponding genes causing the phenotypic variation. Reverse genetic screens have been employed as a way to circumvent this issue, but can often be limited in scope. Here we demonstrate an innovative approach to gene discovery. Using *C. elegans* as a model system, we used a whole-genome sequenced multi-mutation library, from the Million Mutation Project, together with the Sequence Kernel Association Test (SKAT), to rapidly screen for and identify genes associated with a phenotype of interest, namely defects in dye-filling of ciliated sensory neurons. Such anomalies in dye-filling are often associated with the disruption of cilia, organelles which in humans are implicated in sensory physiology (including vision, smell and hearing), development and disease. Beyond identifying several well characterised dye-filling genes, our approach uncovered three genes not previously linked to ciliated sensory neuron development or function. From these putative novel dye-filling genes, we confirmed the involvement of BGNT-1.1 in ciliated sensory neuron function and morphogenesis. BGNT-1.1 functions at the *trans*-Golgi network of sheath cells (glia) to influence dye-filling and cilium length, in a cell non-autonomous manner. Notably, BGNT-1.1 is the orthologue of human B3GNT1/B4GAT1, a glycosyltransferase associated with Walker-Warburg syndrome (WWS). WWS is a multigenic disorder characterised by muscular dystrophy as well as brain and eye anomalies. Together, our work unveils an effective and innovative approach to gene discovery, and provides the first evidence that B3GNT1-associated Walker-Warburg syndrome may be considered a ciliopathy.

Author Summary

Model organisms are useful tools for uncovering new genes involved in a biological process *via* genetic screens. Such an approach is powerful, but suffers from drawbacks that can slow down gene discovery. In forward genetics screens, difficult-to-map phenotypes present daunting challenges, and whole-genome coverage can be equally challenging for reverse genetic screens where typically only a single gene's function is assayed per strain. Here, we show a different approach which includes positive aspects of forward (high-coverage, randomly-induced mutations) and reverse genetics (prior knowledge of gene disruption) to accelerate gene discovery. We paired a whole-genome sequenced multi-mutation *C. elegans* library with a rare-variant associated test to rapidly identify genes associated with a phenotype of interest: defects in sensory neurons bearing sensory organelles called cilia, *via* a simple dye-filling assay to probe the form and function of these cells. We found two well characterised dye-filling genes and three genes, not previously linked to ciliated sensory neuron development or function, that were associated with dye-filling defects. We reveal that disruption of one of these (BGNT-1.1), whose human orthologue is associated with Walker-Warburg syndrome, results in abrogated uptake of dye and cilia length defects. We believe that our novel approach is useful for any organism with a small genome that can be quickly sequenced and where many mutant strains can be easily isolated and phenotyped, such as *Drosophila* and *Arabidopsis*.

Introduction

A powerful, tried and true approach to identify which genes function in a particular biological process is to create collections of organisms harbouring multiple mutations *via* random mutagenesis, followed by screening the mutant library for organisms that exhibit the desired altered phenotypes. Although such forward genetics strategies have produced numerous fundamental discoveries, a significant limitation of this approach in metazoans is the prolonged time required to identify the causative mutations. The bottleneck typically arises from the required genetic mapping, complementation tests to exclude known genes, and sequencing of candidates genes.

To circumvent the major disadvantage of forward genetics, reverse genetic approaches have been employed. Various strategies for disrupting a collection of known genes (*e.g.,* RNAi, homologous recombination, transposon mutagenesis, *etc.*) are combined with phenotypic screening to identify candidates. Reverse genetics approaches also have drawbacks, however, including the need to handle and process tens of thousands of strains to assay the entire genome, off-target effects in the case of RNAi, and omission of essential genes.

We hypothesised that we could use whole-genome sequencing in combination with statistical genetics to inaugurate a novel gene discovery approach which retains the advantages of both forward and reverse genetics, and yet minimises their downsides. To do this, we employed the Million Mutation Project (MMP) [1], a collection of 2007 *Caenorhabditis elegans* strains harbouring randomly-induced mutations whose genomes are fully sequenced (data is publicly available: http://genome.sfu.ca/mmp/about.html). This mutant library represents an unprecedented genetic resource for any multicellular organism, wherein the strains collectively

95 contain one or more potentially disruptive alleles affecting nearly all *C. elegans* coding
96 regions. On average, each strain contains ~ 400 non-synonymous mutations affecting protein
97 coding sequences.
98
99 We postulated that this whole-genome sequence information would allow an "eyes wide
100 open" approach when performing a genetic screen, such that pairing this resource with a high-
101 throughput assay would enable rapid discovery of genes not previously associated with our
102 biological process of interest. Here, we demonstrate that testing for association between variants
103 from the MMP library and phenotype data with the Sequence Kernel Association test (SKAT)
104 [2] allows us to effectively and efficiently predict novel genes important for our chosen
105 biological process: the development and function of the amphid and phasmid sensillum, which
106 includes both ciliated sensory neurons as well as glial-like neuronal support cells.
107
108 Primary (non-motile) cilia arise from a modified centriole (basal body) and act as
109 'cellular antennae' that transduce environmental cues to the cell [3]. They enable sensory
110 physiology (such as olfaction/chemosensation, mechanosensation, vision) and are central to
111 signalling pathways essential for metazoan development [4]. Dysfunction of cilia is implicated
112 in a number of human diseases, including polycystic kidney disease, congenital heart disease,
113 and an emerging group of genetic disorders termed ciliopathies (*e.g.*, Bardet-Biedl, Meckel-
114 Gruber and Joubert Syndromes). In these ciliopathies, disruption of many, if not all, cilia in the
115 human body results in a plethora of defects, including retinal degeneration, organ cyst formation,
116 obesity, brain malformations, and various other ailments [5][6].
117

In *C. elegans*, the uptake of a fluorescent lipophilic dye, DiI, from the environment is used to probe the integrity of the amphid and phasmid sensillum, which includes cilia and ciliated sensory neurons, as well as glial-like sheath cells. DiI is selectively incorporated into six pairs of ciliated amphid channel sensory neurons in the head (ADF, ADL, ASH, ASI, ASJ, and ASK), and two pairs of ciliated phasmid channel sensory neurons in the tail (PHA and PHB), *via* environmentally-exposed cilia present at the tips of dendrites (**S1 Fig**) [7,8]. Many dye-filling (*dyf*) mutants known from genetic screens [8,9] harbour mutations in genes influencing ciliated sensory neuron development and function, including ciliogenesis [10], cilia maintenance [11], axon guidance [9], dendrite anchoring/formation [10], as well as cell fate [12]. Importantly, non-cell autonomous effects from disruption of neural support (glial) cells can also result in dye-filling defects [10,13].

When we applied SKAT to the phenotype data we collected from screening the MMP strains for dye-filling, we found that a previously uncharacterized *C. elegans* gene, *bgnt-1.1/F01D4.9*, plays an essential role in this process. We found that the ciliated sensory neurons of *bgnt-1.1* mutants fail to fill with a lipophilic dye, a phenotype indicative their dysfunction, and that BGNT-1.1 localises specifically to the *trans*-Golgi network of the amphid and phasmid sheath cells. These are glial-like neuronal support cells, which are critical for the development and function of ciliated sensory neurons. Interestingly, *bgnt-1.1* is the orthologue of human B3GNT1/B4GAT1, a gene implicated in Walker-Warburg syndrome [14,15], a disorder with clinical ailments resembling a ciliary disease (ciliopathy).

Results

We screened 480 randomly-chosen whole-genome sequenced multi-mutation MMP strains, ~25% of the library, for defects in DiI uptake in amphid and phasmid ciliated sensory neurons (**Fig 1**). We found 40 MMP strains which exhibit significant amphid dye-filling defects and 40 MMP strains which exhibit significant phasmid dye-filling defects; the strains with amphid and phasmid dye-filling defects are not necessarily identical (**Fig 1C, Table 1, S1 Table**).

Table 1. Summary of dye-fill phenotype classes observed

Phenotype summary	Number of strains
Amphid and phasmid dye-fill defect	11
Amphid and phasmid partial dye-fill defect	12
Phasmid only partial dye-fill defect	17
Amphid only partial dye-fill defect	17
Wild-type dye-filling	423

Fig 1. Dye-filling (ciliated sensory neuron development/function) screening methodology and results. (A, B) Input to the screen was 480 whole genome-sequenced multi-mutant strains from the Million Mutation Project [10]. Mixed-stage *C. elegans* cultures were incubated with DiI for 30 minutes, washed in buffer and then examined by fluorescence microscopy for their ability to uptake the dye into head (amphid) and tail (phasmid) sensory neurons. (C) Dye-filling phenotypes of each of the 480 MMP strains which were assayed. The proportion of worms exhibiting dye-filling in strains represented by dark grey diamonds were not statistically separable from the proportion of wild-type worms exhibiting dye-filling as assessed by a Fisher's exact test with p-values adjusted for a 5% false discovery rate (Benjamini–Hochberg procedure) to control for multiple testing. Blue and red diamonds represent strains with mainly or exclusively amphid or phasmid dye-filling defects, while purple diamonds show strains with

161 defects in both amphid and phasmid sensory neurons. Two highlighted strains, VC20615 and
162 VC20628, contain mutations which alter conserved amino acid residues in the protein encoded
163 by *C. elegans bgnt-1.1,* a gene identified by SKAT to be associated with both amphid and
164 phasmid dye-filling defects.
165
166 We identified 11 completely dye-fill defective strains, where all worms sampled failed to
167 take up dye. A preliminary look at the data indicates that of these, 10 contained deleterious
168 ("knockout") mutations in previously identified dye-filling genes (*e.g.*, nonsense and frameshift-
169 inducing deletions; **S2 Table**). Additionally, we uncovered 47 partially dye-fill defective strains,
170 where a proportion of the population failed to fill with dye significantly more often than wild-
171 type worms. Of these partially dye-fill defective strains, 1 harbours a nonsense mutation and 10
172 display missense mutations in known dye-filling genes (**S2 Table**).
173
174 Despite the fact that we can identify some strains with mutations in genes previously
175 shown to cause dye-filling defects, it is not clear that it is the mutations in these genes which are
176 necessarily the cause of the dye-filling defects in these strains. Furthermore, there are 38 strains
177 where we cannot even generate a hypothesis as to what genetic variation is responsible for the
178 dye-filling defect. To facilitate identification of genes responsible for the observed dye-fill
179 defects, we hypothesised that a recently developed statistical genetics approach commonly used
180 in human genetics, but under-utilised in model organisms, would allow for the rapid
181 prioritisation of candidate genes. Specifically we chose to employ the sequence kernel
182 association test (SKAT) to uncover genes associated with the dye-filling phenotype. SKAT is a
183 regression method to test for association between rare and/or common genetic variants in a
184 region and a continuous or dichotomous trait [2].

185

186 We chose SKAT over other statistical analyses for several reasons. For our dataset, it was
187 imperative that we chose an association test that dealt effectively with rare variants, as
188 800,000/850,000 of the non-synonymous variants in the MMP library are unique; meaning that
189 they are present in only a single isogenic strain in the library. Hence, genome-wide association
190 study (GWAS) approaches, which typically test for an association between common variants
191 (generally defined as a minor allele frequency > 5%) and a trait of interest, would be unsuitable
192 for analysis of phenotype datasets derived from the MMP library. We also viewed SKAT as an
193 optimal method to use for our dataset because it permits the use of prior information to assign
194 weights to genetic variants. For example, nonsense mutations might be expected to be more
195 deleterious than other variants which may cause more modest changes to the protein, such as
196 missense mutations and in-frame deletions. The C-alpha test [16], which is quite similar to
197 SKAT in the absence of covariants (*e.g.,* age, sex, *etc.*), could have also been used for our
198 dataset, but we chose to employ SKAT because it facilitates implementing and assigning
199 biologically relevant weights to variants. Finally, SKAT was chosen over other related burden
200 tests, such as the cohort allelic sums test (CAST) [17] and the combined multivariate and
201 collapsing (CMC) method [18], because unlike these tests, SKAT does not assume that all
202 (common) variants will affect the trait in the same direction.

203

204 Given that the groups of worms which have amphid dye-filling and phasmid dye-filling
205 defects do not necessarily overlap, we performed SKAT separately for each dataset. We chose to
206 perform the linear regression version of SKAT in combination with log transformation of the
207 response (phenotype) variable, as opposed to a logistic regression version of SKAT because in
208 its current implementation, the logistic regression version of SKAT does not work with

209 proportion data, and takes only dichotomous traits coded as 0 or 1. Quantile-quantile (QQ)-plots
210 were used to choose the appropriate constant to add to the response (phenotype) variable before
211 log transformation (**S2 & S3 Fig**). Finally, we performed SKAT with biologically relevant
212 weights assigned to the variants. We assigned mutations which would likely result in the creation
213 of a null mutation (nonsense and splicing mutations, as well as frameshift causing deletions) a
214 weight of 1, mutations which would result in truncation of the protein (in-frame deletions) a
215 weight of 0.75, and mutations which would result in a change in amino acid sequence (missense
216 mutation) a weight of 0.25. We hypothesised these were reasonable weights to assign to each
217 class of mutation based on the current knowledge in the field of genetics.
218
219 Genome-wide SKAT analyses using biologically relevant weights on the amphid dye-
220 filling dataset reveal 5 genes that reach significance when we adjust for multiple testing using a
221 false discovery rate (FDR; Benjamini-Hochberg procedure) of 5% (FDR adjusted p-value was <
222 0.05, **Table 2**, **S3 Table**). SKAT analyses using biologically relevant weights on the phasmid
223 dye-filling dataset uncovered 3 genes which reached significance, again using a FDR of 5%
224 (FDR adjusted p-value was < 0.05, **Table 3**, **S4 Table**). Dye-filling defects of both amphid and
225 phasmid ciliated neurons is significantly associated with genes encoding intraflagellar transport
226 proteins (OSM-1 and CHE-3), and a glycosyltransferase (BGNT-1.1; **Table 2 and 3**). Amphid-
227 specific dye-filling defects are found to be associated with genes encoding an Arf-GAP related
228 protein, CNT-1, as well as a mitotic spindle assembly checkpoint protein, MDF-1 (**Table 2**). No
229 gene was found to be significantly associated with only phasmid dye-filling defects (**Table 2 and**
230 **Table 3**).

Table 2. Genes with genome-wide significance for amphid ciliated neuron dye-filling phenotypes, ordered by FDR adjusted p-value.

Gene	Sequence	p-value	FDR adjusted p-value	# variants	Human homologue	function	ciliated sensory neuron evidence	*C. elegans* ciliated neuron expression
osm-1	T27B1.1	1.0E-06	0.001	14	IFT172	Intraflagellar Transport complex B component	Perkins et al., 1986; Signor et al., 1999	yes
che-3	F18C12.1	1.6E-05	0.009	21	DYNC2H1	Intraflagellar Transport dynein heavy chain	Perkins et al., 1986; Signor et al., 1999	yes
bgnt-1.1	F01D4.9	5.6E-05	0.02	7	B3GNT1	Glycoslytransferase		unknown
mdf-1	C50F4.11	1.0E-04	0.03	8	MAD1	Mitotic spindle assembly checkpoint protein		unknown
cnt-1	Y17G7B.15	1.2E-04	0.03	8	ACAP2	Arf-GAP		unknown

248 **Table 3. Genes with genome-wide significance for phasmid ciliated neuron dye-filling phenotypes, ordered by FDR adjusted p-value.**

249

Gene	Sequence	p-value	FDR adjusted p-value	# variants	Human homologue	function	ciliated sensory neuron evidence	*C. elegans* ciliated neuron expression
osm-1	T27B1.1	2.7E-06	0.003	14	IFT172	Intraflagellar Transport (IFT) complex B component	Perkins et al., 1986; Signor et al., 1999	yes
bgnt-1.1	F01D4.9	1.4E-05	0.008	7	B3GNT1	Glycoslytransferase		unknown
che-3	F18C12.1	3.6E-05	0.01	21	DYNC2H1	IFT dynein heavy chain	Perkins et al., 1986; Signor et al., 1999	yes

Of the three genes associated with both amphid and phasmid dye-filling defects, namely *osm-1*, *che-3*, and *bgnt-1.1*, the first two are well characterised genes whose dye-filling defective phenotypes are ascribed to their key roles in intraflagellar transport (IFT). OSM-1 is the orthologue of mammalian IFT172, an IFT-B subcomplex component which functions as an adaptor to link ciliary cargo (*e.g.,* tubulin, receptors and signaling molecules) to the anterograde IFT kinesin motors, and is necessary for ciliogenesis [10]. CHE-3, the orthologue of mammalian DYNC2H1, is a cytoplasmic dynein heavy chain which powers the retrograde IFT-dynein motor. This molecular motor recycles IFT machinery from the growing ciliary tip back to the ciliary base and is also necessary for proper cilium formation/maintenance [19,20]. These two known dye-fill/cilia genes represent excellent positive controls for our screen, and indicate that other genes found to be significantly associated with these phenotypes may be novel dye-fill genes that influence cilia function.

Interestingly, one of the other amphid dye-filling gene hits, *cnt-1*, encodes a protein that play roles in membrane trafficking/dynamics by influencing small GTPase function, *via* GTPase-activating protein or GAP activity. The general involvement of small GTPases of the Arf, Arf-like (Arl) and Rab families in cilium formation/development is well established [3]. *cnt-1* encodes the orthologue of human ACAP2, which interacts with both Rab35 [21] and Arf6 [22] to mediate crosstalk between these two proteins, at least in the context of PC12 cell neurite outgrowth, and potentially through endocytic recycling [23]. Another amphid dye-filling gene hit, *mdf-1*, is homologous to *Mad1*, and encodes a Mitotic spindle assembly checkpoint protein [24]. To the best of our knowledge, our findings are the first to directly implicate *mdf-1/Mad1* as being important for cilia development and/or function but other Mitotic spindle assembly

checkpoint proteins have previously been linked to cilia, including BUBR1 [25] and APC-Cdc20 [26].

The third, putative novel dye-filling gene significantly associated with both amphid and phasmid dye-fill phenotypes is *bgnt-1.1* (**Table 2 & 3, S3 and S4 Table**). *bgnt-1.1* encodes an unstudied *C. elegans* glycosyltransferase 49 family member homologous to human B3GNT1/B4GAT1 (**S4 Fig**). B3GNT1 catalyses the addition of β1–3 linked N-acetylglucosamine to galactose [27]. In HeLa cells, its subcellular localisation is concentrated at the *trans*-Golgi [28]. B3gnt1 knockout mice exhibit axon guidance phenotypes [29,30] and deficient behavioural responses to estrous females [31]. In humans, mutations in B3GNT1 are associated with a congenital muscular dystrophy with brain and eye anomalies, Walker-Warburg syndrome (WWS) [14,15]. WWS is a suspected, but unconfirmed ciliopathy; it exhibits 6 core features common to ciliopathies, including Dandy-Walker malformation, hypoplasia of the corpus callosum, mental retardation, posterior encephalocele, retinitis pigmentosa and *situs inversus* [5]. Additionally, one patient is reported to exhibit dysplastic kidneys [14], a developmental disruption which leads to cyst formation, illuminating a potential 7th core ciliopathy feature to this disorder, renal cystic disease. To divulge a potential connection between B3GNT1 and cilia and/or ciliated sensory neuron function, we sought to confirm the role of *C. elegans* BGNT-1.1 in dye-filling, and analyse its involvement role in ciliated sensory neuron development.

Of the eight MMP strains harbouring mutations in *bgnt-1.1*, three (VC20615, VC20628 and VC20326) exhibited severe dye-fill phenotypes (**S1 Table**). The C -> T missense mutation in *bgnt-1.1* in VC20615 corresponds to P194S alteration in the protein sequence, while VC20628

297 and VC20326 each harbour an identical G -> A missense mutation in *bgnt-1.1*, which leads to a
298 G205E amino acid change in the protein sequence. Both of these mutations alter conserved
299 amino acid residues (**S5 Fig**). In the screen we encountered 5 additional strains that harboured
300 missense mutations in *bgnt-1.1* but did not exhibit dye-filling defects. Close examination of the
301 predicted effects of these missense mutations on the amino acid sequence of the protein indicates
302 that these alleles do not lead to amino acid changes in conserved residues (**S5 Fig**), and thus it is
303 not surprising that these strains do not exhibit dye-fill defects.
304
305 To confirm that the mutations in *bgnt-1.1* was responsible for the dye-filling phenotypes
306 in *bgnt-1.1* mutants, we rescued the dye-fill defects by expressing a fosmid containing a wild-
307 type copy of *bgnt-1.1* in an extrachromosomal array (**Fig 2**). Another way to confirm that
308 disruption of *bgnt-1.1* causes dye-fill defects would be to observe this phenotype in a strain
309 harbouring a knock-out mutation in *bgnt-1.1*. Although there are 49 *bgnt-1.1* alleles available, a
310 knock-out allele of *bgnt-1.1* did not yet exist. There are two insertion/deletion alleles available,
311 *gk1221* and *tm4314*, but both fall within introns and thus unlikely to affect protein function.
312 Thus, we also tested the causality of *bgnt-1.1 via* a relatively efficient SNP mapping approach.
313 We established that the dye-fill phenotypes from VC20615 and VC20628 strains map to the
314 *bgnt-1.1* locus, on chromosome IV between -5 cM and 8 cM (**S6 Fig**). Notably, in both VC20615
315 and VC20628 strains, *bgnt-1.1* was the only gene in this region harbouring a mutation which was
316 common to both of these strains.
317
318 **Fig 2. Confirmation of *bgnt-1.1* as a novel dye-filling gene.** (A) Wild-type *bgnt-1.1* rescues
319 dye-filling defects in *bgnt-1.1 (gk361915)* mutants. Transformation of VC20628 *bgnt-1.1*
320 *(gk361915)* with a fosmid containing wild-type *bgnt-1.1* (WRM065bB05) completely rescues the

amphid, and partially rescues the phasmid dye-filling defects of VC20628 *bgnt-1.1 (gk361915)* mutants, as assessed by fluorescence microscopy. (B) Quantitation of amphid and phasmid dye-filling in the mutant strain VC20628 in the presence or absence of a fosmid rescue contruct ($p < 0.05$, Fisher's exact test). Error bars represent 95% confidence intervals (Pearson Clopper method).

Finally, we used CRISPR-Cas9 genome engineering [32] to independently generate three *bgnt-1.1* knockout alleles. All three alleles delete the first and second exon of *bgnt-1.1* and insert a selectable marker, P*myo-2*::GFP, in their place. When tested for dye-filling defects, we observe an identical dye-filling phenotype as observed in the 6X outcrossed *bgnt-1.1 (gk210889)* G205E allele from the Million Mutation Project (**Fig 3**). In all of these mutants, we observe a great decrease in the amount of dye that enters the amphid ciliated sensory neurons, which is often undetectable, as well as a complete absence of dye-filling of the phasmid ciliated sensory neurons. Together, these findings indicate that loss of *bgnt-1.1* function results in dye-filling defects.

Fig 3. CRISPR-Cas9 knockout of *bgnt-1.1* causes dye-filling defects. (A) three *bgnt-1.1* knockout alleles, independently generated via CRISPR-Cas9, exhibit amphid and phasmid (B) dye-fill defects compared to wild-type worms ($p < 0.0001$, Fisher's exact test, p-values adjusted for a 5% false discovery rate using the Benjamini–Hochberg procedure). The magnitude of the dye-filling defects in the CRISPR-Cas9 knockout alleles is similar to that observed in the MMP *bgnt-1.1 gk210889* missense mutation, which results in G205E amino acid change. Error bars represent 95% confidence intervals (Pearson Clopper method). (C) Representative images of

dye-filling in wild-type (N2), three CRISPR-Cas9-generated *bgnt-1.1* knockout alleles and the MMP *bgnt-1.1 gk210889* missense mutation allele.

To shed light on how *bgnt-1.1* affects dye-filling, we studied expression of GFP-tagged BGNT-1.1 constructed *via* fosmid recombineering (https://transgeneome.mpi-cbg.de/transgeneomics/index.html), and thus containing all of this gene's endogenous regulatory elements. We observed that in *C. elegans*, the protein localises to discrete structures in the cell body of the amphid and phasmid glial-like sheath cells (AMsh and PHsh, respectively) in the head and tail of the animal (**Fig 4a**). These cells are intimately associated with the ciliated sensory neurons in the pore region where cilia are exposed to the external environment (**Fig S1**).

Fig 4. BGNT-1.1 localises to the trans-golgi in the amphid and phasmid sheath cells. (A) BGNT-1.1::GFP generated from a recombineered fosmid localises to the amphid and phasmid sheath cells. Amphid ciliated neurons (ADF, ADL, ASH, ASI, ASJ, and ASK) were visualized with DiI, while phasmid ciliated neurons (PHA and PHB) were visualized with P*osm-5*::XBX-1::tdTomato. Amphid sheath cells are abbreviated to AMsh, and phasmid shearh cells are abbreviated to PHsh. (B) BGNT-1.1::GFP localises proximal to the discrete anti-SQL-1 puncta. SQL-1 is an established *cis*-Golgi marker, indicating that BGNT-1.1 is concentrated at the *trans*-Golgi. (C) ADL cilia are significantly longer in *bgnt-1.1* mutants compared to wild-type ($p < 0.01$, Kruskal-Wallis test). ADL cilia are labelled with P*srh-220*::IFT-20::tdTomato. IFT-20 (IFT20) localises to cilia basal bodies (bb) and axonemes. The *srh-220* promoter drives expression primarily in ADL neurons.

Mammalian B3GNT1 is found at the *trans*-Golgi network in HeLa cells [28]. To assess whether this is also where *C. elegans* BGNT-1.1 localises, we performed antibody staining for SQL-1, an established *cis*-Golgi marker [33], in the strain expressing BGNT-1.1::GFP. We observe that in both the head and tail, the localisation of BGNT-1.1::GFP is always proximal to the discrete SQL-1 puncta, indicating that *C. elegans* BGNT-1.1 is concentrated at the *trans*-Golgi, as expected (**Fig 4b**).

Next, we queried whether loss of *bgnt-1.1* function in the amphid and phasmid sheath cells leads to any gross ciliary morphology defects by expressing a ciliary marker in *bgnt-1.1* mutants, namely the GFP-tagged IFT-B subcomplex protein, CHE-2 (IFT80). This experiment indicates that although the cilia of *bgnt-1.1* mutants fail to fill with dye, their ciliary structures appear superficially wild-type (**S7A Fig**). Since modest cilia structure defects may be more difficult to observe using pan-cilia markers, due to overlapping ciliary signals, we also characterised the phenotype of cilia and dendrites in *bgnt-1.1* mutants within a single ciliated amphid cell, the ADL neuron. For this purpose, we used the primarily cell-specific ADL promoter, P*srh-220*, to drive expression of another cilia marker, IFT-20 (IFT20) tagged with tdTomato. In this strain, we also expressed cytoplasmic GFP in the amphid socket cells so that we could evaluate whether or not the ADL cilia were correctly associated with the surrounding glial support cells and the pore where DiI has access to the amphid ciliated sensory neurons from the environment. Similar to the experiment with the CHE-2::GFP pan-cilia marker, the P*srh-220*::IFT-20::tdTomato marker revealed that the ADL cilia and amphid socket (Amso) cell morphology also appear superficially wild-type in *bgnt-1.1* mutants (**S7B Fig**). We then sought to assay for potential phenotypes involving ADL cilia length (**Fig 4c**); length of socket cell penetration by ADL (proxied by the distance from the distal tip of ADL cilia to the distal end of

391 the socket cell tip; **S7C Fig)**; ADL guidance (proportion of double rod cilia/amphid; **S7D Fig**);
392 and finally, ADL dendrite blebbing (structural alteration where dendrites take bead on a string
393 appearance; **S7E Fig**). Our analyses reveal that ADL cilia in *bgnt-1.1* mutants are wild-type in
394 most aspects except for a modest cilia length defect. Specifically, *bgnt-1.1* mutants were
395 observed to have significantly longer cilia compared to wild-type worms (**Fig 4c**; $p < 0.01$,
396 Kruskal-Wallis test).
397
398 BGNT-1.1 therefore influences amphid and phasmid neuron development and function,
399 as well all modestly affects cilium length, without overtly affecting the gross structure of neurons
400 or cilium formation. The localisation of BGNT-1.1 at the *trans*-Golgi network of sheath cells
401 signifies that its effect on ciliated sensory neurons is non-cell autonomous. Interestingly, when
402 the *bgnt-1.1* amphid ciliated sensory neurons do fill with dye, we observe bright accumulations
403 of dye along and/or beside the dendrites (**Fig 3c**). These are often brighter than the staining of the
404 cell bodies. Accumulations of dye have been observed in wild-type worms and have been
405 attributed to the dye-filling of the amphid sheath cells [34], but these are qualitatively much
406 smaller than what we observed in the *bgnt-1.1* mutants. This suggests a potential alteration in the
407 ability of the sheath cell to take up, or intracellularly distribute dye when BGNT-1.1 is disrupted.
408
409 In humans, mutations in *B3GNT1* cause Walker-Warburg syndrome. Given that mutations in
410 B3GNT1 lead to WWS and that it is classified as a dystroglycanopathy, a group of muscular
411 disorders whose etiology is hypothesised to be caused by aberrant glycosylation of dystroglycan,
412 we tested whether or not the *C. elegans* dystroglycan homologs, *dgn-1, dgn-2* and *dgn-3*,
413 exhibited dye-filling phenotypes. We observed that all *dgn* mutants exhibited dye-filling
414 indistinguishable from wild-type worms (**S9 Fig**), indicating that BGNT-1.1 function in dye-

415 filling is likely independent of dystroglycan. Interestingly, as highlighted earlier, the WWS
416 congenital muscular dystrophy exhibits 6 features beyond muscle structure/function disruption
417 which are core ciliary disorder (ciliopathies) features [5]. Our findings that *C. elegans bgnt-1.1* is
418 expressed in glial cells directly associated with, and necessary for the function of ciliated sensory
419 neurons, is consistent with its role in cilium-dependent dye-filling.
420

Discussion

Here we demonstrate that rare-variant association analysis (*e.g.,* SKAT) is an efficient way to rapidly uncover novel genes for a phenotype of interest (*e.g.*, ciliated sensory neuron function) in whole-genome sequenced strains harbouring multiple mutations induced *via* random mutagenesis. We found that three cilia-related genes, *osm-1*, *che-3* and *bgnt-1.1* were significantly associated with dye-filling defects, suggesting that the remaining unstudied genes, *cnt-1* and *mdf-1*, likely represent genes important for ciliary/sensory neuron development and/or function.

The glycosyltransferase BGNT-1.1 is essential for ciliated sensory neuron dye-filling and cilium length control

We confirmed that *bgnt-1.1,* a gene identified by SKAT as being associated with the dye-filling phenotypes but not previously implicated in cilia or amphid-sensillum function, is a *bona fide* dye-filling gene. We observed that: *(1)* two missense mutations in *bgnt-1.1* result in severe dye-fill defects in three MMP strains, and three CRISP-Cas9-mediated *bgnt-1.1* gene disruptions also cause dye-fill defects; *(2)* a fosmid containing full-length wild-type *bgnt-1.1* rescues the dye-filling phenotype in *bgnt-1.1* mutants; *(3)* the dye-filling phenotypes in the MMP strains with mutations in *bgnt-1.1* map to the *bgnt-1.1* locus; *(4)* BGTN-1 is expressed in sheath cells, which are directly implicated in dye-filling; and finally; and *(5)* mutations in *bgnt-1.1* result in a small but statistically significant ciliary length defect. Together, these data strongly indicate that BGNT-1.1, which we find localises as expected to the *trans*-Golgi network, functions in sheath (glia-like) cells to influence dye-filling.

Considerations of our novel gene discovery approach

The power of genome-wide rare-variant association analysis (*e.g.,* SKAT) augments as the number of strains increases (the probability of additional mutations in specific genes is increased), and thus, screening the entire MMP library would likely uncover many additional genes associated with dye-filling defects. To try to assess the minimal number of strains that should be assayed with this approach we performed a power analysis. Raw amphid dye-filling phenotype and genotype data was randomly sub-sampled (without replacement) and analysis was performed via SKAT with, and without, biologically relevant weights. This was done 100 times for each sample size (50, 100, 200, 300, 400). For each sample size, power was calculated as the proportion of times the analysis found at least one gene to be significantly associated with the phenotype. We observed that there was 40% power to detect a single gene as being associated with the amphid dye-filling phenotype at N = 400 for both SKAT with and without biologically relevant weights (**S9 Fig**). Thus, we recommend that future studies using this method should use a sample size close to what was used in this present study (~ 500) to maximize the probability that a gene(s) will be found that is significantly associated with the phenotype of interest.

We performed SKAT analyses *via* two methods, 1) while applying biologically relevant weights to the variants (**S3 & S4 Tables**), and 2) while weighting all variants equally (**S5 & S6 Tables**). SKAT analysis of the 480 strains without weights was less powerful, and resulted in identifying only 3 genes as being significantly associated with the amphid dye-filling phenotype and 1 gene as being significantly associated with the phasmid dye-filling phenotype; compared to 5 genes and 3 genes, respectively, when biologically relevant weights were used. Although there appears to be no difference in power when SKAT is performed with or without weights at smaller sample sizes (**S9 Fig**). Thus, to maximize the ability to detect genes associated with the

phenotype of interest, in addition to recommending a minmum sample size of ~ 500, we also recommend assigning biologically relevant weights when using SKAT with the MMP library. The weight assignment could be simple, as done here, or more complex, calculating, for example, the SIFT [35] or Polyphen-2 [36] scores for assessing the severity of each variant in the MMP library.

The genome-wide statistical genetic approach presented here has several advantages over traditional screening approaches. It generates a prioritised list of candidate genes likely responsible for the phenotype of interest. After this list is generated *via* screening and SKAT analysis, candidates can be tested for their causality of the phenotype through several standard genetic approaches in *C. elegans*. Candidates could be confirmed, for example, by *(i)* testing for the phenotype in knock-out mutants or RNAi; *(ii)* genetic rescue experiments; *(iii)* performing a genetic complementation test between two loss of function alleles; or, *(iv)* mapping the mutation to the gene locus. This strategy may work for phenotypes where the traditional polymorphic SNP-mapping strain, CB4856, diverges from the reference wild-type strain, N2, from which the MMP library was generated [1], as well as partially-penetrant or other difficult-to-score phenotypes. In the case of *bgnt-1.1*, we performed genetic rescue experiments, SNP mapping and created CRISPR-Cas9 knockout strains to support our the SKAT findings, which together confirm that *bgnt-1.1* mutations cause dye-filling defects.

Another potential extension and utility of this approach that could work for some (non-neural) phenotypes would be pairing the screening of the MMP strains with RNAi to look for enhancing, suppressing or synthetic phenotypes, and then using SKAT to prioritise a list of candidate genes. Furthermore, as more data from multiple phenotypes are collected on the MMP

494 strains, these could be combined to perform multi-variate genome-wide statistical analysis on
495 whole-genome sequence data. Such approaches are more powerful than univariate approaches in
496 the case of SNP array data [37–39], and such tests can also indicate which variants are
497 pleiotropic, or specific to a single phenotype. How to perform this multivariate phenotype
498 analysis on whole-genome sequences is currently an active area of research and tools to make
499 this possible are being developed, with [40] looking promising.
500
501 There are also challenges and limitations to the statistical genetic approach presented
502 here. First, this approach of performing a "medium"-scale screen of the MMP strains is limited
503 to assays that can be done without genetic manipulation of the strains. For example, introducing
504 a functional 'reporter' (transgene) into 480 strains would require a prohibitive amount of work,
505 although this has been done for 90 MMP strains [41]. Second, the statistical analysis presented
506 here is only possible for genes which have > 1 variant in the population of worms screened. In
507 practice, we found it works optimally for strains with at least 7 variants. This is due to the
508 distribution of p-values when attempting to control for multiple testing; in our dataset, fewer than
509 7 variants led to a skewed p-value distribution and an inflation of False-discovery rate adjusted
510 p-values. This strict rule demanding high-coverage for our SKAT analysis leads to only 1150
511 genes in the 480 MMP strains being considered here. This is due to the distribution of variant
512 counts per gene in the MMP strains (**S9 Fig**), which exponentially decreases from 1 to N.
513
514
515 **Mechanism of BGNT-1.1 in dye-filling**
516
517 How disrupting BGNT-1.1 abrogates dye filling remains uncertain. One possibility is that
518 the glycosyltransferase regulates the association of cilia with the sheath and socket glial-like
519 cells which envelop them (**S1 Fig**). Specifically, we hypothesise that BGNT-1.1 functions in the

trans-golgi network of the amphid and phasmid sheath to glycosylate key unidentified proteins important for the association of this sensillum organ. This defect will not be visible at the level of light microscopy, and could perhaps result from changes to the lamellar membrane that surround the amphid/phasmid cilia, or the secreted extracellular material lining these channels. Which substrate(s) the β1,3-N-acetylglucosaminyltransferase, BGNT-1.1 (B3GNT1), glycosylates, and how this influences sensory neuron/glial cell development and function, remains to be determined in a future, detailed study of the gene.

Conclusion

In conclusion, we demonstrated the utility and efficiency of using deep-sequenced multi-mutant strains in combination with SKAT to rapidly uncover novel genes required for a biological process of interest—here, ciliated sensory neuron development and/or function. The role of BGNT-1.1 in this process, seemingly independent of dystroglycan, supports the notion that Walker-Warburg syndrome may result at least in part from ciliary dysfunction, and thus could be considered a novel ciliopathy. Our findings also underscore the importance of identifying novel dye-filling genes, some of which might be implicated in human ciliopathies. For all new putative dye-filling genes highlighted in this study, we had no prior knowledge of their importance in ciliated sensory neuron function, and may not have (easily) uncovered them using alternative methods. Our approach therefore reduces the hurdle of traditional forward genetic methods, namely identifying the causative allele, and improves upon reverse genetics by allowing high gene/mutation coverage in a relatively small number of strains. Lastly, we propose that our approach is applicable not only for *C. elegans*, but any organism with a small genome that can be quickly sequenced and where numerous mutant strains can be isolated and

544 phenotyped with relative ease, including *Drosophila* and *Arabidopsis.*

545

546

Materials and Methods

Strains and maintenance

Worms were cultured on Nematode Growth Medium (NGM) seeded with Escherichia coli (OP50) at 20ºC as described previously [42]. The following strains were obtained from the Caenorhabditis Genetics Center (University of Minnesota, Minneapolis, MN): N2 Bristol, CB4856, CH1869, CH1878 and PR813. VC2010, the wild-type reference strain used during the dye-filling screen, was derived from N2 [43]. The Million Mutation Project strains were isolated and their genomes' sequenced by Thompson *et al*. [1]. The 480 Million Mutation Project strains used in this study are listed in **S1 Table**.

Preparation of transgenic lines

For native rescue of VC20628 *bgnt-1.1(gk361915)*, 25 ng/µl of fosmid WRM065bB05 containing *bgnt-1.1* was injected into *bgnt-1.1* mutants along with 80 ng/µl of pRF4 *rol-6(su1006dm)* as a co-injection marker. *bgnt-1.1(gk361915)*; Ex[CHE-2::GFP; pRF4] was created by crossing *bgnt-1.1(gk361915)* with wild-type worms expressing Ex[CHE-2::GFP; pRF4]. The translational P*srh-220*::IFT-20::tdTomato fusion was generated as described in [11], except that tdTomato was used in place of GFP. 1 µl of the PCR product was microinjected into germline of gravid worms along with a co-injection markers (pRF4 *rol-6*(*su1006dm*), final concentration of 100 ng/µl). Stable lines expressing this extrachromosomal array were crossed into DM13283 *dpy-5(e907)*; sIs12964[P*grd-15*::GFP; pCeh361] to create the strain MX1924 *dpy-5(e907)*; Ex[P*srh-220*::IFT-20::tdTomato; pRF4]; sIs12964[P*grd-15*::GFP; pCeh361]. *bgnt-1.1(gk361915)* was also introduced to this line *via* genetic crossing to create MX2236 *bgnt-1.1(gk361915); dpy-5(e907)*; Ex[P*srh-220*::IFT-20::tdTomato; pRF4]; sIs12964[P*grd-15*::GFP; pCeh361]. The BGNT-1.1::GFP recombineered fosmid construct (Construct #

571 6821068113870966 H08) was obtained from the TransgeneOme (https://transgeneome.mpi-
572 cbg.de/transgeneomics/index.html). To generate a strain expressing this construct, 25 ng/µl of the
573 BGNT-1.1::GFP recombineered fosmid was injected into N2 worms along with 4 ng/ul of Posm-
574 5::XBX-1::tdTomato as a cilia-marker, and 80 ng/µl of pRF4 *rol-6(su1006dm)* as a co-injection
575 marker.
576
577 **CRISPR-Cas9 knockout mutant strain generation.**
578 VC3671 (*gk3637*), VC3674 (*gk3674*), and VC3675 (*gk3639*) for *bgnt-1.1*/*F01D4.9* were
579 generated using the CRISPR-Cas9 system as described by [32] in an N2 VC2010 background
580 [1]. The 20 bp guide sequence for *bgnt-1.1* was designed to include a 3'GG motif, as guides with
581 GG at the 3' end are purported to give higher integration efficiency [44]. 500 bp homology arms
582 (ordered as gBlocks from IDT) were designed to flank exons 1 and 2 of *bgnt-1.1*. The homology
583 arms were inserted into a P*myo-2*::GFP-neoR-loxP disruption/deletion vector (provided by the
584 Calarco Lab) using Gibson Assembly. The guide sequence and homology arms sequences are
585 available in **S7 Table** and **S8 Table**, respectively.
586
587 Of the three null mutations, *gk3637* was generated using purified Cas9 protein, while
588 *gk3674* and *gk3639* were generated using a plasmid-encoded version of the protein. The Cas9
589 protein was prepared according to the procedure described in [45] Paix et al. (2015). The protein
590 injection mix was assembled as described in [45] and used tracrRNA and *bgnt-1.1* crRNA
591 ordered from IDT.
592
593 Putative integrants were validated by generating PCR amplicons spanning the junction
594 between genomic DNA and the inserted cassette. Primer F01D4.9-1-L was used in conjunction

595 with primer pMyo-2-SEC to validate the region just upstream of the putative insertion. This
596 generated a 1075 bp product that covers genomic DNA as well as a region within the insertion.
597 Primer F01D4.9-1-R was used in conjunction with primer NeoR-SEC to validate the region just
598 downstream of the putative insertion. This generated a 1632 bp product that covers genomic
599 DNA as well as a region within the insertion. Sanger sequencing of the PCR amplicons was
600 conducted by the Nucleic Acid Protein Service Unit (NAPS, UBC).
601

602 **Identification, mapping and cloning of bgnt-1.1**

603 To rough-map the dye-filling defects of Million Mutation Project strains to an arm of a
604 chromosome we used the high-throughput SNP mapping approach created by Davis *et al*. . The
605 following SNPs used by Davis *et al*. [46] were omitted from our analysis because the whole
606 genome sequence data from Thompson *et al.* [1] could not safely deduce that the SNPs from
607 parental strain subjected to mutagenesis, VC2010 (from which the Million Mutation Project
608 strains were generated), matched those of Bristol N2 but not Hawaiin CB4856 (mapping strain):
609 W03D8, F58D5, T01D1, Y6D1A, Y38E10A, T12B5, R10D12, F11A1, and T24C2.
610

611 **Dye-filling procedures**

612 Dye-filling assays were performed using the fluorescent dye DiI (Molecular Probes;
613 DiIC18 Vybrant DiI cell-labelling solution, diluted 1:1000 with M9 buffer). Mixed stage *C.*
614 *elegans* cultures were stained for 30 minutes, and Dil uptake into the amphid and phasmid
615 neurons was visualised using either a Zeiss fluorescent dissection scope (dye-filling screen) or
616 spinning disc confocal microscope (WaveFX spinning disc confocal system from Quorum
617 Technologies) using a 25X oil (N.A 0.8) objective and Hammamatsu 9100 EMCCD camera.
618 Volocity software (PerkinElmer) was used for acquisition. The completely dye-filling defective

(*dyf*) mutant strain PR813 *osm-5(p813)* was used as a positive control for the dye-filling phenotype.

For the dye-filling screen, two plates of mixed-stage *C. elegans* were dye-filled for each Million Mutation Project strain, and defects were quantified by counting the number of worms exhibiting amphid and/or phasmid dye-filling defects. A worm was classified to have a dye-filling defect if: *i)* no fluorescence was observed, *ii)* fluorescence was observed to be greatly reduced (minimum of an estimated 3x fluorescence reduction compared to wild-type staining from the experiment at the same magnification and laser intensity) and/or *iii)* fluorescence staining pattern was abrogated (*e.g.*, accumulations of fluorescence at tips of dendrites with little to no staining in cell bodies). Fifteen worms were scored from each plate. If the dye-filling of a Million Mutation Project strain appeared qualitatively dimmer than wild-type worms across both plates or if ≥ 25% of the population exhibited a dye-filling defect the assay was repeated for that strain. A Fisher's exact test followed by p-value adjustment using false discovery rate of 5% (Benjamini–Hochberg procedure) was used to if they exhibited a significant dye-fill defect compared to wild-type (N2). This was done separately for both amphids and phasmids.

Imaging sensory neurons and cilia

For visualisation of fluorescent-tagged proteins, worms were immobilised in 1µl of 25mM levamisole and 1µl of 0.1µm diameter polystyrene microspheres (Polysciences 00876-15, 2.5% w/v suspension) on 10% agarose pads and visualised under a spinning disc confocal microscope (WaveFX spinning disc confocal system from Quorum Technologies) using a 100X oil (N.A 1.4) objective and Hammamatsu 9100 EMCCD camera. Volocity 6.3 was used to deconvolve images as well as measure ADL cilia length and distal tip of ADL cilia to distal end

643 of amphid socket cell length. The researcher was blind while performing the quantisation of
644 ADL cilia/dendrite phenotypes.
645

646 **Immunofluorescence**

647 Worms were permeabilised, fixed and stained according to standard methods [47]. To
648 mark the *cis*-Golgi, two anti-SQL-1 antibodies, one directed against the N terminus of SQL-1
649 and one affinity purified antibody against the C terminus of SQL-1, were used. These antibodies
650 have been characterised previously [33]. Both were visualised with secondary goat-anti rabbit
651 Alexa 594 (Molecular Probes, Eugene, OR; 1:800). Localisation of BGNT-1::GFP and SQL-1
652 was imaged using a SpinD1454 Roper/Nikon spinning disk microscope with a 100x objective.
653
654
655
656

657 **SKAT analysis**

658 We performed SKAT using the SKAT package (version 1.0.9) [2] in R (version 3.2.4).
659 No covariates were used. Given that the MMP library was created *via* random mutagenesis of the
660 same isogenic parental strain [1] we did not have to control for population stratification. We
661 chose to perform SKAT using a linear regression framework to take full advantage of the
662 proportion data we had collected, as the logistic regression framework for SKAT only allows for
663 a dichotomous response variable. To apply a linear regression framework to our proportion data
664 we added a small constant to all the data points for the response variable, and then log
665 transformed them. We used probability plots to choose the best constant (**S2 & S3 Fig**), and thus

666 used a constant of 0.005 for the amphid phenotype data, and a constant of 0.05 for the phasmid
667 phenotype data.

668 Custom, biologically relevant weights were assigned to the variants. Nonsense, splicing
669 mutations and frameshift causing deletions were assigned a weight of 1, in-frame deletions were
670 assigned a weight of 0.75, and missense mutations were assigned a weight of 0.25. Gene-based
671 tests for all genes with a minor allele count > 6 were performed. A false discovery rate
672 (Benjamini-Hochberg procedure) of 5% was used to determine genes which were significantly
673 associated with the phenotype. Make, Bash, Perl and R scripts used to perform the analysis can
674 be found at: https://github.com/ttimbers/Million-Mutation-Project-dye-filling-SKAT.git

675

676 **Power analysis**

677 To estimate power and recommend a minimum sample size for future experiments we
678 performed a bootstrap power analysis using the amphid dataset. To do this, we randomly
679 sampled (resampling = FALSE) N strains from the dataset we collected, and performed the
680 SKAT analysis presented in this paper. We did this 100 times for N = 50, 100, 200, 300 and 400.
681 We then estimated power as the proportion of times we observed a gene to be significantly
682 associated with the phenotype. This was also done for two, three, four and five genes. The code
683 used to perform this analysis can also be found in the Github repository for this study:
684 https://github.com/ttimbers/Million-Mutation-Project-dye-filling-SKAT.git

685

686 **Phylogenetic Analysis**

687 Protein sequences (obtained from: http://www.cazy.org/) were aligned using MUSCLE
688 3.7 [48]. The phylogenetic tree was built using PhyML 3.0 aLRT [49] and viewed using FigTree

689 version 1.3.1 (http://tree.bio.ed.ac.uk/software/figtree/).

690

691

692

693

694 **Acknowledgements**

695 T.A.T. acknowledges a Banting Postdoctoral Fellowship from the Canadian Institutes of
696 Health Research (CIHR). M.R.L. acknowledges funding from CIHR (MOP82870) and a senior
697 scholar award from Michael Smith Foundation for Health Research (MSFHR). The work in the
698 D.G.M. laboratory was supported by CIHR. D.G.M. is a Senior Fellow of the Canadian Institute
699 For Advanced Research. S.J.G. acknowledges funding from a Natural Sciences and Engineering
700 Research Council (NSERC) Undergraduate Student Research Award (USRA).

701

References

1. Thompson O, Edgley M, Strasbourger P, Flibotte S, Ewing B, Adair R, et al. The million mutation project: a new approach to genetics in Caenorhabditis elegans. Genome Res. 2013;23: 1749–1762. doi:10.1101/gr.157651.113

2. Wu MC, Lee S, Cai T, Li Y, Boehnke M, Lin X. Rare-variant association testing for sequencing data with the sequence kernel association test. Am J Hum Genet. 2011;89: 82–93. doi:10.1016/j.ajhg.2011.05.029

3. Sung C-H, Leroux MR. The roles of evolutionarily conserved functional modules in cilia-related trafficking. Nat Cell Biol. 2013;15: 1387–1397. doi:10.1038/ncb2888

4. Veland IR, Awan A, Pedersen LB, Yoder BK, Christensen ST. Primary cilia and signaling pathways in mammalian development, health and disease. Nephron Physiol. 2009;111: p39–53. doi:10.1159/000208212

5. Baker K, Beales PL. Making sense of cilia in disease: the human ciliopathies. Am J Med Genet C Semin Med Genet. 2009;151C: 281–295. doi:10.1002/ajmg.c.30231

6. Hildebrandt F, Benzing T, Katsanis N. Ciliopathies. N Engl J Med. 2011;364: 1533–1543. doi:10.1056/NEJMra1010172

7. Perkins LA, Hedgecock EM, Thomson JN, Culotti JG. Mutant sensory cilia in the nematode Caenorhabditis elegans. Dev Biol. 1986;117: 456–487.

8. Starich TA, Herman RK, Kari CK, Yeh WH, Schackwitz WS, Schuyler MW, et al. Mutations affecting the chemosensory neurons of Caenorhabditis elegans. Genetics. 1995;139: 171–188.

9. Hedgecock EM, Culotti JG, Thomson JN, Perkins LA. Axonal guidance mutants of Caenorhabditis elegans identified by filling sensory neurons with fluorescein dyes. Dev Biol. 1985;111: 158–170.

10. Inglis PN, Ou G, Leroux MR, Scholey J. The sensory cilia of Caenorhabditis elegans_Revised. WormBook. 2007; doi:10.1895/wormbook.1.126.2

11. Mohan S, Timbers TA, Kennedy J, Blacque OE, Leroux MR. Striated rootlet and nonfilamentous forms of rootletin maintain ciliary function. Curr Biol CB. 2013;23: 2016–2022. doi:10.1016/j.cub.2013.08.033

12. Herman MA, Horvitz HR. The Caenorhabditis elegans gene lin-44 controls the polarity of asymmetric cell divisions. Dev Camb Engl. 1994;120: 1035–1047.

13. Oikonomou G, Shaham S. The glia of Caenorhabditis elegans. Glia. 2011;59: 1253–1263. doi:10.1002/glia.21084

14. Buysse K, Riemersma M, Powell G, van Reeuwijk J, Chitayat D, Roscioli T, et al. Missense mutations in β-1,3-N-acetylglucosaminyltransferase 1 (B3GNT1) cause Walker-Warburg syndrome. Hum Mol Genet. 2013;22: 1746–1754. doi:10.1093/hmg/ddt021

15. Shaheen R, Faqeih E, Ansari S, Alkuraya FS. A truncating mutation in B3GNT1 causes severe Walker-Warburg syndrome. Neurogenetics. 2013;14: 243–245. doi:10.1007/s10048-013-0367-8

16. Neale BM, Rivas MA, Voight BF, Altshuler D, Devlin B, Orho-Melander M, et al. Testing for an unusual distribution of rare variants. PLoS Genet. 2011;7: e1001322. doi:10.1371/journal.pgen.1001322

17. Morgenthaler S, Thilly WG. A strategy to discover genes that carry multi-allelic or mono-allelic risk for common diseases: a cohort allelic sums test (CAST). Mutat Res. 2007;615: 28–56. doi:10.1016/j.mrfmmm.2006.09.003

18. Li B, Leal SM. Methods for detecting associations with rare variants for common diseases: application to analysis of sequence data. Am J Hum Genet. 2008;83: 311–321. doi:10.1016/j.ajhg.2008.06.024

19. Signor D, Wedaman KP, Orozco JT, Dwyer ND, Bargmann CI, Rose LS, et al. Role of a class DHC1b dynein in retrograde transport of IFT motors and IFT raft particles along cilia, but not dendrites, in chemosensory neurons of living Caenorhabditis elegans. J Cell Biol. 1999;147: 519–530.

20. Wicks SR, de Vries CJ, van Luenen HG, Plasterk RH. CHE-3, a cytosolic dynein heavy chain, is required for sensory cilia structure and function in Caenorhabditis elegans. Dev Biol. 2000;221: 295–307. doi:10.1006/dbio.2000.9686

21. Kanno E, Ishibashi K, Kobayashi H, Matsui T, Ohbayashi N, Fukuda M. Comprehensive screening for novel rab-binding proteins by GST pull-down assay using 60 different mammalian Rabs. Traffic Cph Den. 2010;11: 491–507. doi:10.1111/j.1600-0854.2010.01038.x

22. Jackson TR, Brown FD, Nie Z, Miura K, Foroni L, Sun J, et al. ACAPs are arf6 GTPase-activating proteins that function in the cell periphery. J Cell Biol. 2000;151: 627–638.

23. Kobayashi H, Fukuda M. Rab35 regulates Arf6 activity through centaurin-β2 (ACAP2) during neurite outgrowth. J Cell Sci. 2012;125: 2235–2243. doi:10.1242/jcs.098657

24. Kitagawa R, Rose AM. Components of the spindle-assembly checkpoint are essential in Caenorhabditis elegans. Nat Cell Biol. 1999;1: 514–521. doi:10.1038/70309

25. Miyamoto T, Porazinski S, Wang H, Borovina A, Ciruna B, Shimizu A, et al. Insufficiency of BUBR1, a mitotic spindle checkpoint regulator, causes impaired ciliogenesis in vertebrates. Hum Mol Genet. 2011;20: 2058–2070. doi:10.1093/hmg/ddr090

26. Wang W, Wu T, Kirschner MW. The master cell cycle regulator APC-Cdc20 regulates ciliary length and disassembly of the primary cilium. eLife. 2014;3: e03083.

27. Zhou D, Berger EG, Hennet T. Molecular cloning of a human UDP-galactose:GlcNAcbeta1,3GalNAc beta1, 3 galactosyltransferase gene encoding an O-linked core3-elongation enzyme. Eur J Biochem FEBS. 1999;263: 571–576.

776 28. Lee PL, Kohler JJ, Pfeffer SR. Association of beta-1,3-N-acetylglucosaminyltransferase 1
777 and beta-1,4-galactosyltransferase 1, trans-Golgi enzymes involved in coupled poly-N-
778 acetyllactosamine synthesis. Glycobiology. 2009;19: 655–664. doi:10.1093/glycob/cwp035

779 29. Henion TR, Raitcheva D, Grosholz R, Biellmann F, Skarnes WC, Hennet T, et al. Beta1,3-
780 N-acetylglucosaminyltransferase 1 glycosylation is required for axon pathfinding by
781 olfactory sensory neurons. J Neurosci Off J Soc Neurosci. 2005;25: 1894–1903.
782 doi:10.1523/JNEUROSCI.4654-04.2005

783 30. Bless E, Raitcheva D, Henion TR, Tobet S, Schwarting GA. Lactosamine modulates the rate
784 of migration of GnRH neurons during mouse development. Eur J Neurosci. 2006;24: 654–
785 660. doi:10.1111/j.1460-9568.2006.04955.x

786 31. Biellmann F, Henion TR, Bürki K, Hennet T. Impaired sexual behavior in male mice
787 deficient for the beta1-3 N-acetylglucosaminyltransferase-I gene. Mol Reprod Dev. 2008;75:
788 699–706. doi:10.1002/mrd.20828

789 32. Norris AD, Kim H-M, Colaiácovo MP, Calarco JA. Efficient Genome Editing in
790 Caenorhabditis elegans with a Toolkit of Dual-Marker Selection Cassettes. Genetics.
791 2015;201: 449–458. doi:10.1534/genetics.115.180679

792 33. Broekhuis JR, Rademakers S, Burghoorn J, Jansen G. SQL-1, homologue of the Golgi
793 protein GMAP210, modulates intraflagellar transport in C. elegans. J Cell Sci. 2013;126:
794 1785–1795. doi:10.1242/jcs.116640

795 34. Ohkura K, Bürglin TR. Dye-filling of the amphid sheath glia: implications for the functional
796 relationship between sensory neurons and glia in Caenorhabditis elegans. Biochem Biophys
797 Res Commun. 2011;406: 188–193. doi:10.1016/j.bbrc.2011.02.003

798 35. Kumar P, Henikoff S, Ng PC. Predicting the effects of coding non-synonymous variants on
799 protein function using the SIFT algorithm. Nat Protoc. 2009;4: 1073–81.
800 doi:10.1038/nprot.2009.86

801 36. Adzhubei IA, Schmidt S, Peshkin L, Ramensky VE, Gerasimova A, Bork P, et al. A method
802 and server for predicting damaging missense mutations. Nat Methods. 2010;7: 248–249.
803 doi:10.1038/nmeth0410-248

804 37. Ferreira MA, Purcell SM. A multivariate test of association. Bioinformatics. 2009;25: 132–3.
805 doi:10.1093/bioinformatics/btn563

806 38. O'Reilly PF, Hoggart CJ, Pomyen Y, Calboli FC, Elliott P, Jarvelin MR, et al. MultiPhen:
807 joint model of multiple phenotypes can increase discovery in GWAS. PLoS One. 2012;7:
808 e34861. doi:10.1371/journal.pone.0034861

809 39. van der Sluis S, Posthuma D, Dolan CV. TATES: efficient multivariate genotype-phenotype
810 analysis for genome-wide association studies. PLoS Genet. 2013;9: e1003235.
811 doi:10.1371/journal.pgen.1003235

40. Sun J, Oualkacha K, Forgetta V, Zheng H-F, Brent Richards J, Ciampi A, et al. A method for analyzing multiple continuous phenotypes in rare variant association studies allowing for flexible correlations in variant effects. Eur J Hum Genet. 2016; doi:10.1038/ejhg.2016.8

41. Wang X, Liu J, Zhu Z, Ou G. The heparan sulfate-modifying enzyme glucuronyl C5-epimerase HSE-5 controls Caenorhabditis elegans Q neuroblast polarization during migration. Dev Biol. 2015;399: 306–314. doi:10.1016/j.ydbio.2015.01.007

42. Brenner S. The genetics of Caenorhabditis elegans. Genetics. 1974;77: 71–94.

43. Flibotte S, Edgley ML, Chaudhry I, Taylor J, Neil SE, Rogula A, et al. Whole-genome profiling of mutagenesis in Caenorhabditis elegans. Genetics. 2010;185: 431–441. doi:10.1534/genetics.110.116616

44. Farboud B, Meyer BJ. Dramatic enhancement of genome editing by CRISPR/Cas9 through improved guide RNA design. Genetics. 2015;199: 959–971. doi:10.1534/genetics.115.175166

45. Paix A, Folkmann A, Rasoloson D, Seydoux G. High Efficiency, Homology-Directed Genome Editing in Caenorhabditis elegans Using CRISPR-Cas9 Ribonucleoprotein Complexes. Genetics. 2015;201: 47–54. doi:10.1534/genetics.115.179382

46. Davis MW, Hammarlund M, Harrach T, Hullett P, Olsen S, Jorgensen EM. Rapid single nucleotide polymorphism mapping in C. elegans. BMC Genomics. 2005;6: 118. doi:10.1186/1471-2164-6-118

47. Finney M, Ruvkun G. The unc-86 gene product couples cell lineage and cell identity in C. elegans. Cell. 1990;63: 895–905.

48. Edgar RC. MUSCLE: a multiple sequence alignment method with reduced time and space complexity. BMC Bioinformatics. 2004;5: 113. doi:10.1186/1471-2105-5-113

49. Guindon S, Dufayard J-F, Lefort V, Anisimova M, Hordijk W, Gascuel O. New algorithms and methods to estimate maximum-likelihood phylogenies: assessing the performance of PhyML 3.0. Syst Biol. 2010;59: 307–321. doi:10.1093/sysbio/syq010

Supporting information captions

S1 Fig. Schematic of a longitudinal section through the wild-type amphid and phasmid sensillum. (A) The socket and sheath cells form the amphid channel through which the cilia are exposed to the environment. The lipophilic dye, DiI, is also presumed to access the cilia *via* this

channel. Cuticle, continuous with the external surface of the worm, lines the socket channel. Matrix is secreted by the Golgi apparatus of the sheath cell, and fills the space that surrounds the cilia. (B) The phasmid sensillum is organised in the same manner as described for the amphid sensillum.

S2 Fig. QQ-plots of the distribution of p-values calculated with SKAT (with and without weights) using the amphid dye-filing dataset. From these plots we chose to log transform the amphid phenotype data (proportion of dye-filling defects) and to add a constant of 0.005 to all values prior to log transformation.

S3 Fig. QQ-plots of the distribution of p-values calculated with SKAT (with and without weights) using the phasmid dye-filing dataset. From these plots we chose to log transform the phasmid phenotype data (proportion of dye-filling defects) and to add a constant of 0.05 to all values prior to log transformation.

S4 Fig. Phylogenetic tree of glycosyltransferase 49 domain containing proteins. The glycosyltransferase 49 domain containing proteins appear to have radiated in *C. elegans*. BGNT-1.1 is the most basal member of this family, and most closely related to vertebrate B3GNT1/ B4GAT1. Protein sequences (obtained from: http://www.cazy.org/) were aligned using MUSCLE 3.7 (Edgar, 2004), and the phylogenetic tree was built using PhyML 3.0 aLRT (Guindon et al., 2010) and viewed using FigTree version 1.3.1 (http://tree.bio.ed.ac.uk/software/figtree/).

868 **S5 Fig. Multiple sequence alignment of *C. elegans* BGNT-1.1 with homologous**
869 **glycosyltransferase 49 domain containing proteins.** In VC20615 the *bgnt-1(gk355974)*
870 mutation results in P194S at a conserved P (highlighted in pink). In VC20628 *the bgnt-*
871 *1(gk361915)* mutation results in G205E at a conserved E (highlighted in blue). Alignment was
872 performed by L-INS-i MAFFT using BLOSUM62 as a scoring matrix and a gap onset penalty of
873 1.53.
874
875 **S6 Fig. VC20615 and VC20628 dye-fill defects map to the *bgnt-1* locus.** (A) Chromosome
876 SNP mapping of VC20615's dyf phenoype. Each pair of lanes shows results from the SNP at the
877 indicated genetic map position, using DNA template from either worms exhibiting dyf (d) or
878 wild-type (+) dye-filling. Linkage is visible as an increase in the proportion of Bristol N2 DNA
879 in dyf lanes compared to the wild-type lanes, and is visible on ChrIV from -5 to 8. (B)
880 chromosome mapping of VC20628's dyf phenoype. Similar to VC20615, linkage is visible as an
881 increase in the proportion of Bristol N2 DNA in dyf lanes compared to the wild-type lanes, and
882 is visible on ChrIV from -5 to 8. All PCR samples from SNP-mapping of each strain were run on
883 the same large gel from which multiple images were captured to visualize all samples.
884
885 **S7 Fig. Ciliary and socket cell structures in the *bgnt-1* mutant are present and appear**
886 **superficially wild-type.** (A) Both amphid and phasmid cilia appear superficially wild-type.
887 GFP-tagged CHE-2 (mammalian IFT80 orthologue) is used as a pan-cilia marker which localises
888 to the basal bodies (bb) and axonemes. (B) ADL cilia correctly enter the amphid socket (AMso)
889 cells in *bgnt-1.1* mutants. ADL cilia are labelled with P*srh-220*::IFT-20::tdTomato. IFT-20
890 (IFT20) localises to cilia basal bodies (bb) and axonemes. The *srh-220* promoter drives
891 expression primarily in ADL neurons. The amphid socket (AMso) cells are labelled with

892 cytoplasmic GFP driven by an amphid socket specific promoter, *grd-15* (Hunt-Newbury et al.
893 2007). (C) ADL cilia penetrate the sockets cells to an equivalent depth in wild-type and *bgnt-1.1*
894 mutants ($p > 0.05$, Kruskal-Wallis test). (D) ADL cilia/dendrites exhibit no guidance defects in
895 *bgnt-1.1* mutants as assessed by the number of double-rod cilia observed in each amphid when
896 ADL was driven by the primarily ADL specific *srh-220* promoter ($p > 0.05$, Fisher's exact test).
897 Error bars represent 95% confidence intervals (Pearson Clopper method). (E) *bgnt-1.1* mutants
898 do not exhibit a significant increase in the proportion of ADL neurons with dendritic blebbing (p
899 > 0.05, Fisher's exact test). Error bars represent 95% confidence intervals (Pearson Clopper
900 method).
901
902 **S8 Fig. *C. elegans* Dystroglycan homologues, *dgn-1*, *dgn-2* and *dgn-3*, are not required for**
903 **dye-filling of amphid or phasmid ciliated sensory neurons.** *dgn* mutants did not exhibit
904 significant dye-filling defects when compared to wild-type ($p > 0.05$, Fisher's exact test followed
905 by a Bonferroni correction) Error bars represent 95% confidence intervals (Clopper Pearson
906 method).
907
908 **S9 Fig. Power analysis of SKAT analysis of amphid dye-filling data.** Raw amphid dye-filling
909 phenotype and genotype data was randomly sub-sampled (without replacement) and analysis was
910 performed via SKAT with (B), and without (A), biologically relevant weights. This was done
911 100 times for each sample size (50, 100, 200, 300, 400). For each sample size, power was
912 calculated as the proportion of times the analysis found a gene to be significantly associated with
913 the phenotype.
914

S10 Fig. Distribution of variant counts for mutated genes from the 480 strains screened in this study from the Million Mutation project. The majority of genes have only a single mutation in the 480 strains screened.

S1 Table. MMP strains phenotyped for dye-filling defects and their respective phenotypes.

S2 Table. Strains which exhibit a dye-fill defect and the known *dyf* genes which are mutated in these strains.

S3 Table. SKAT analysis of amphid dye-filling phenotype using biologically relevant weights.

S4 Table. SKAT analysis of phasmid dye-filling phenotype using biologically relevant weights.

S5 Table. SKAT analysis of amphid dye-filling phenotype where all variants were weighted equally.

S6 Table. SKAT analysis of phasmid dye-filling phenotype where all variants were weighted equally.

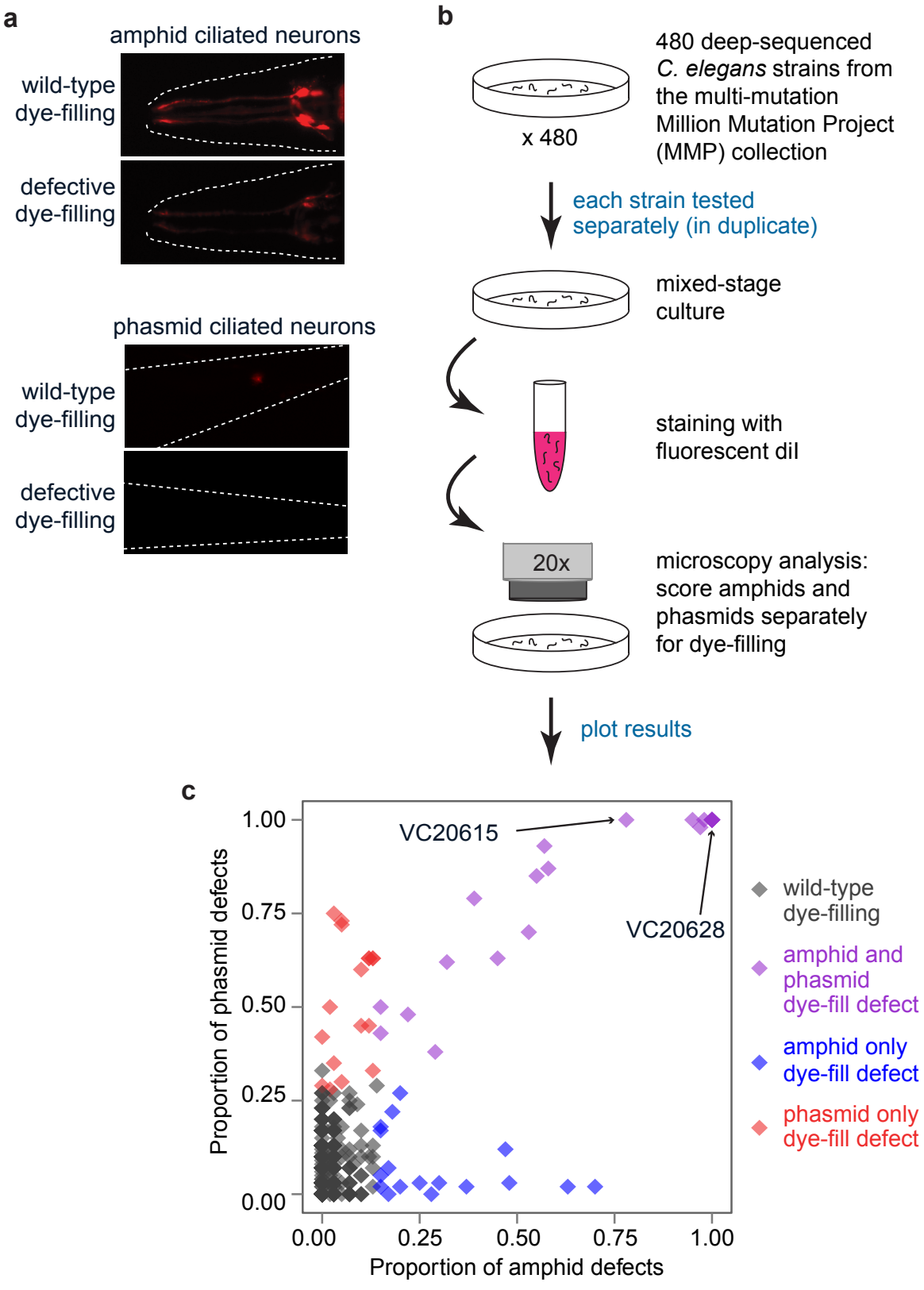

Timbers et al., Figure 1

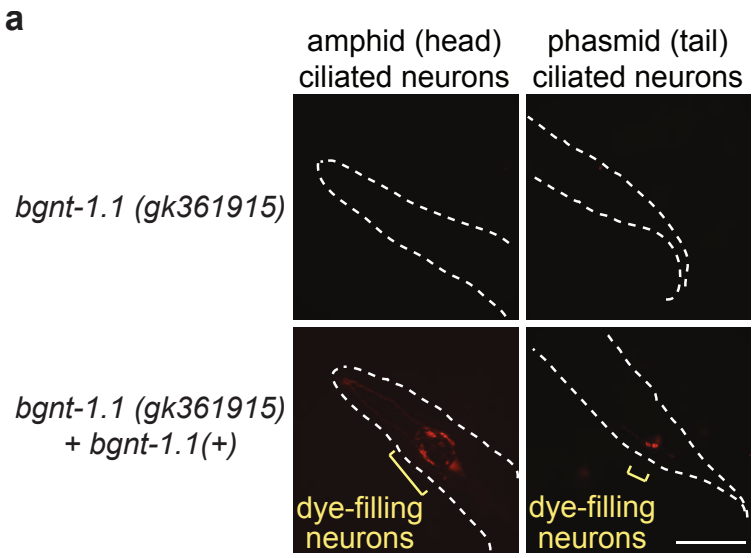

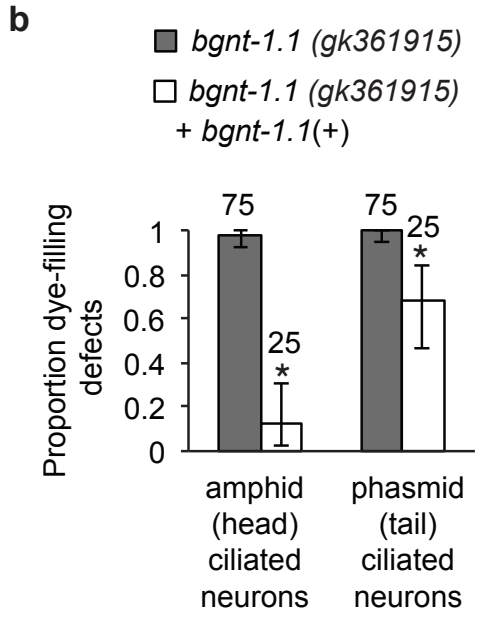

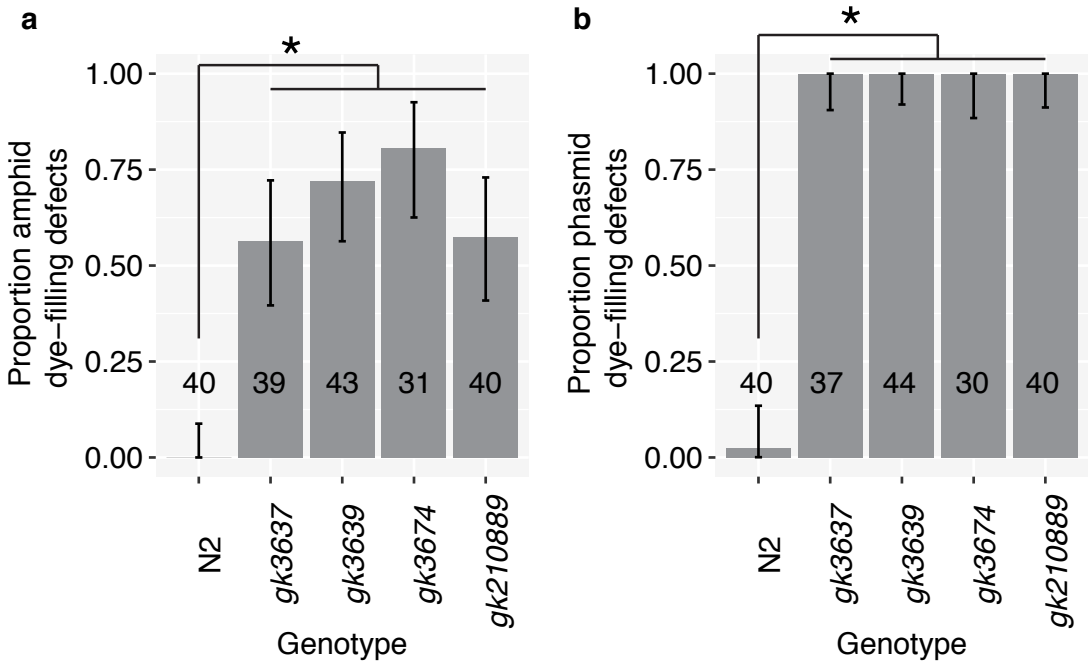

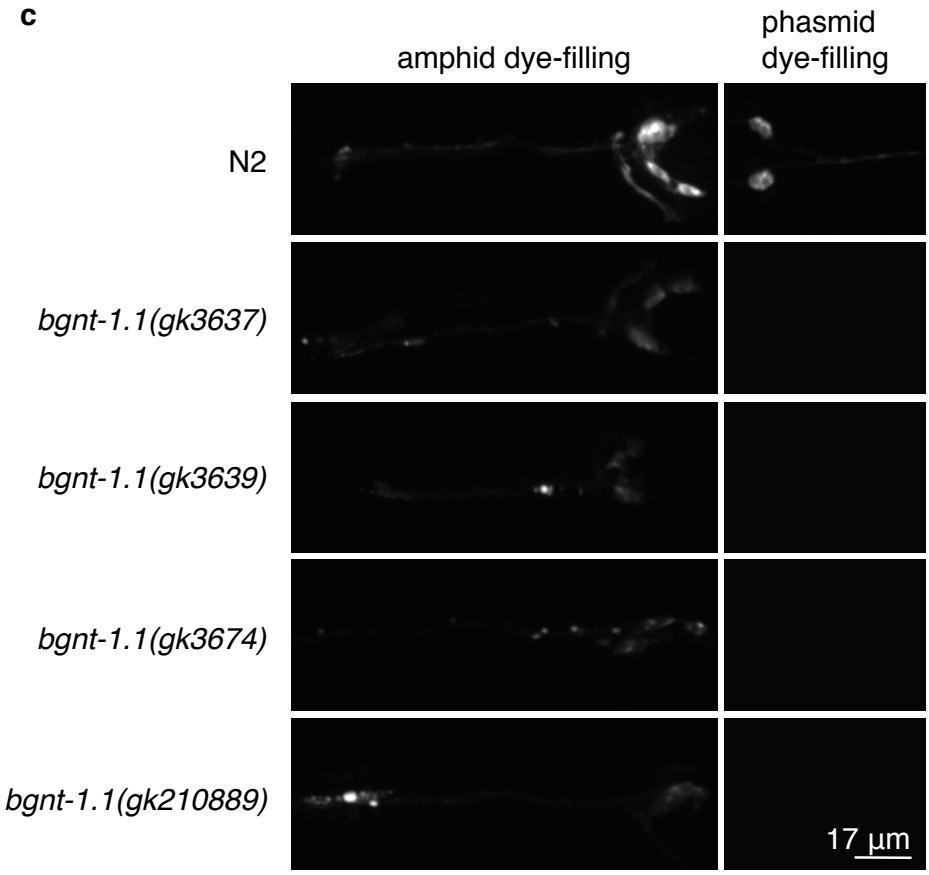

Timbers et al., Figure 3

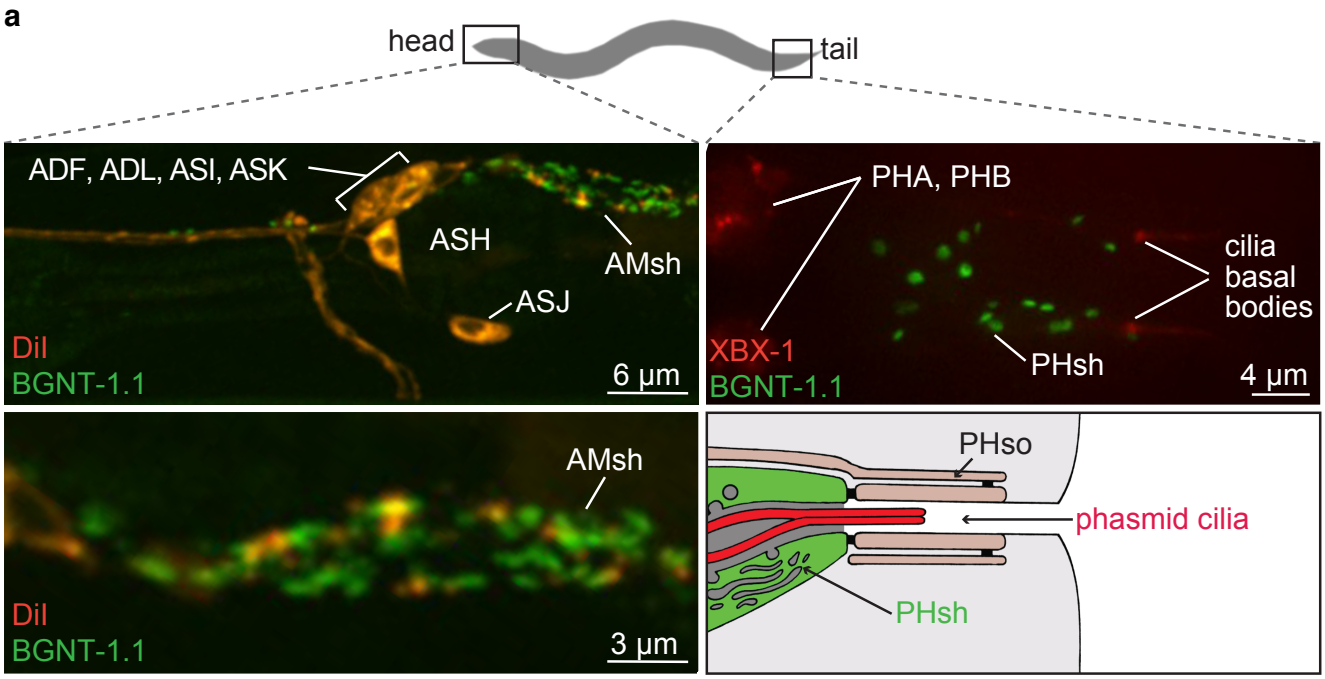

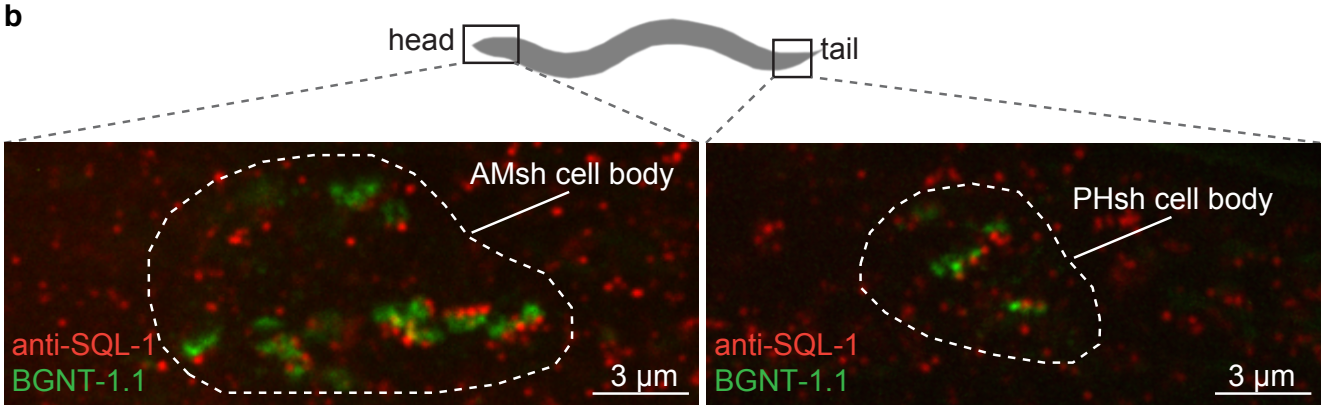

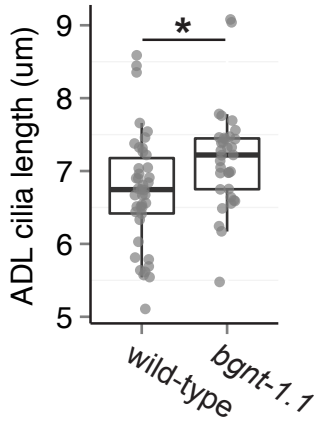

Timbers et al., Figure 4

a

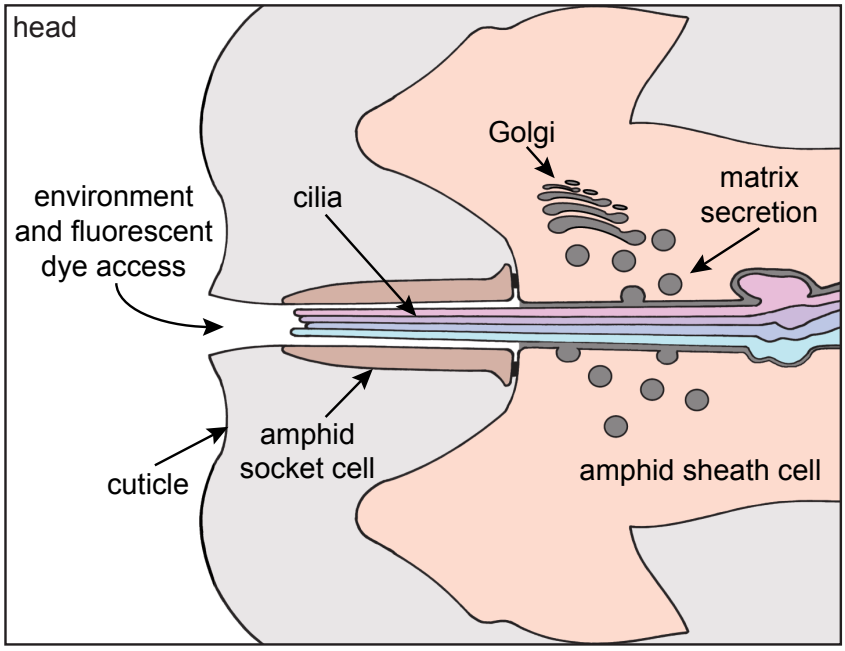

b

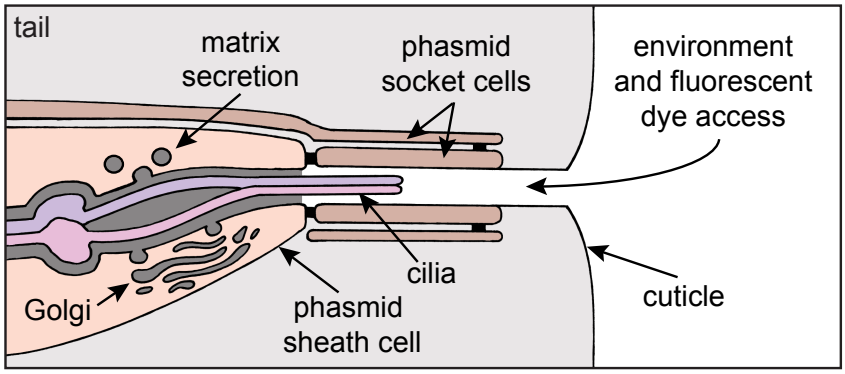

Timbers et al., Figure S1

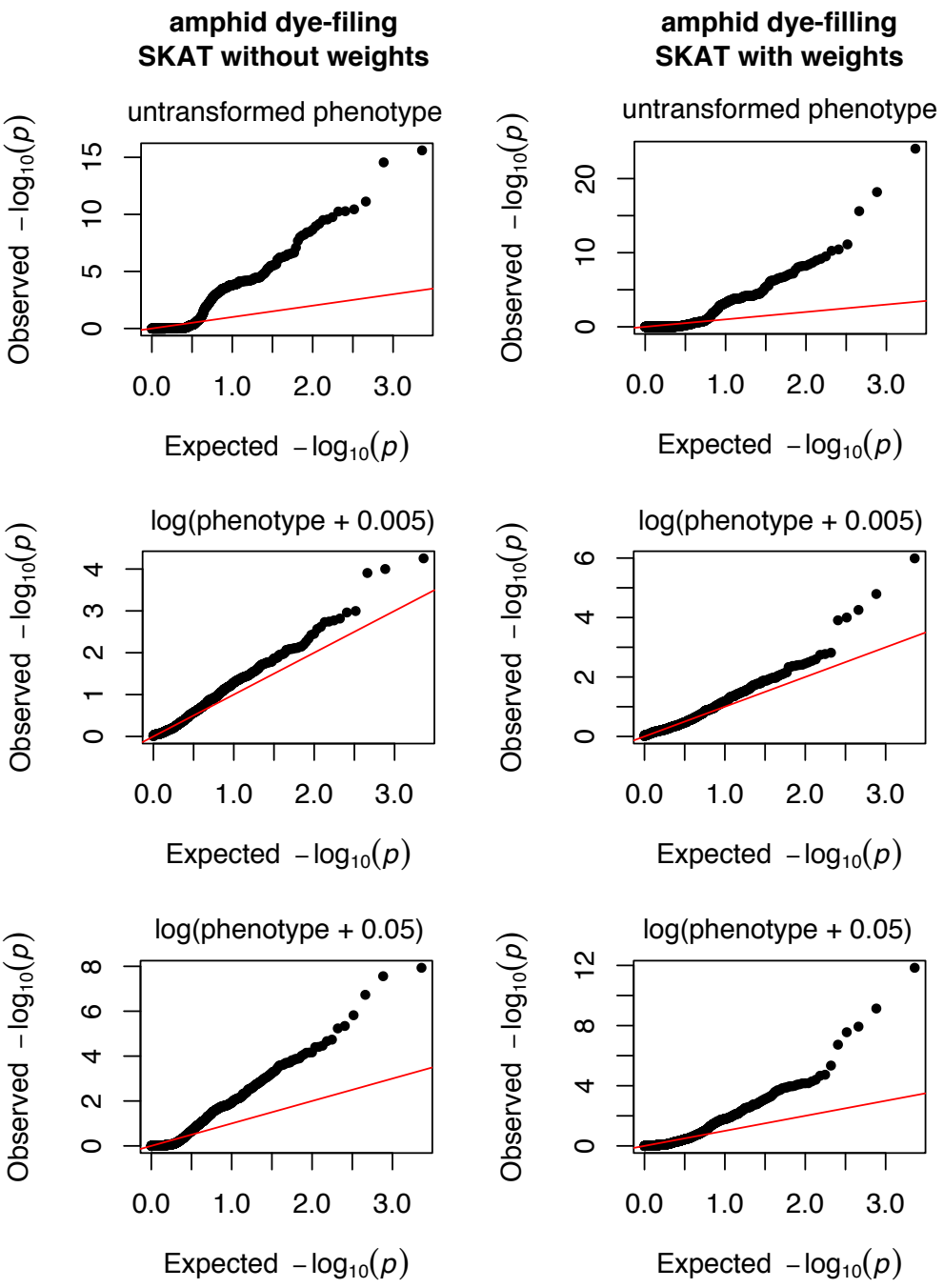

Timbers et al., Figure S2

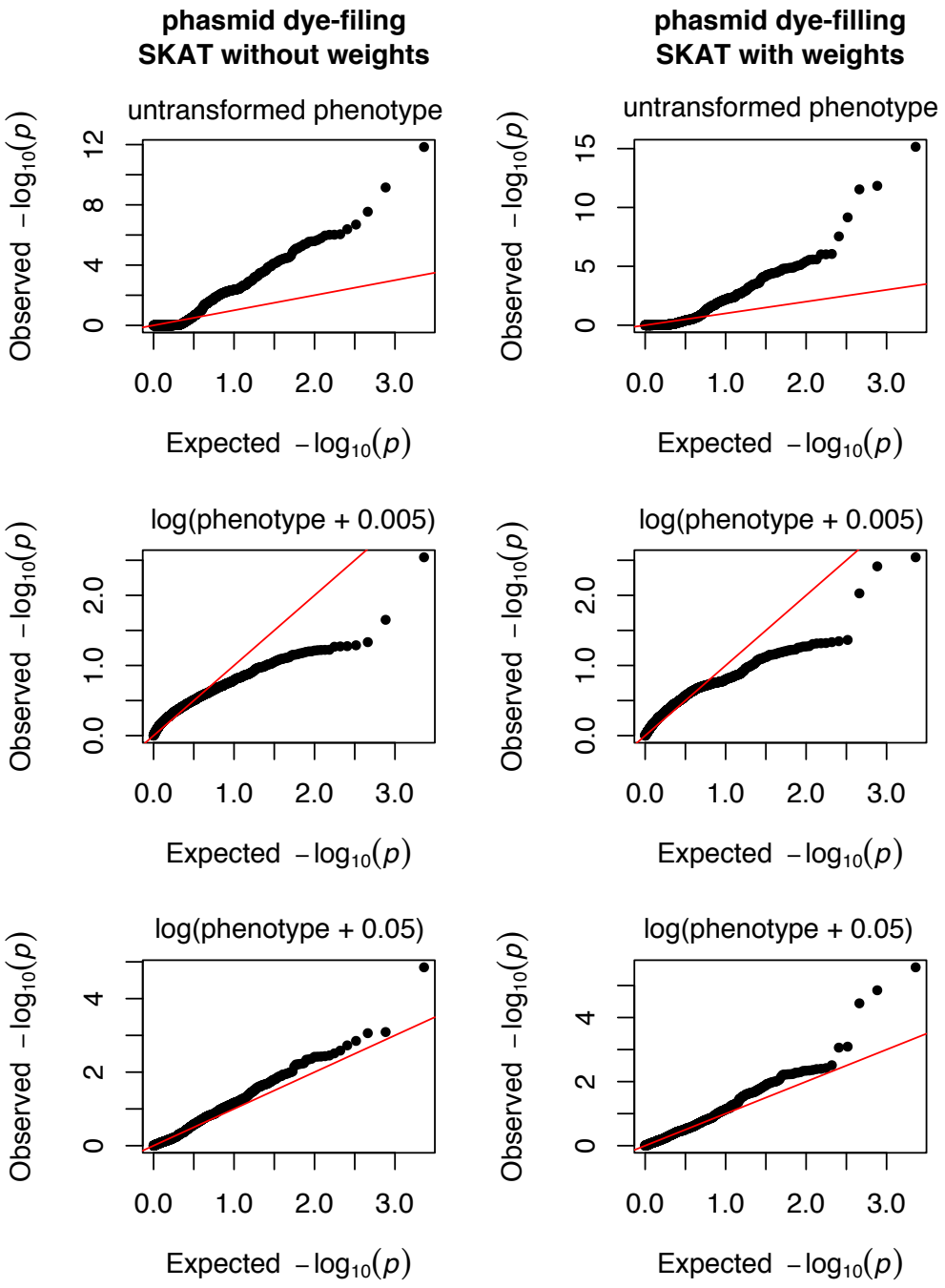

Timbers et al., Figure S3

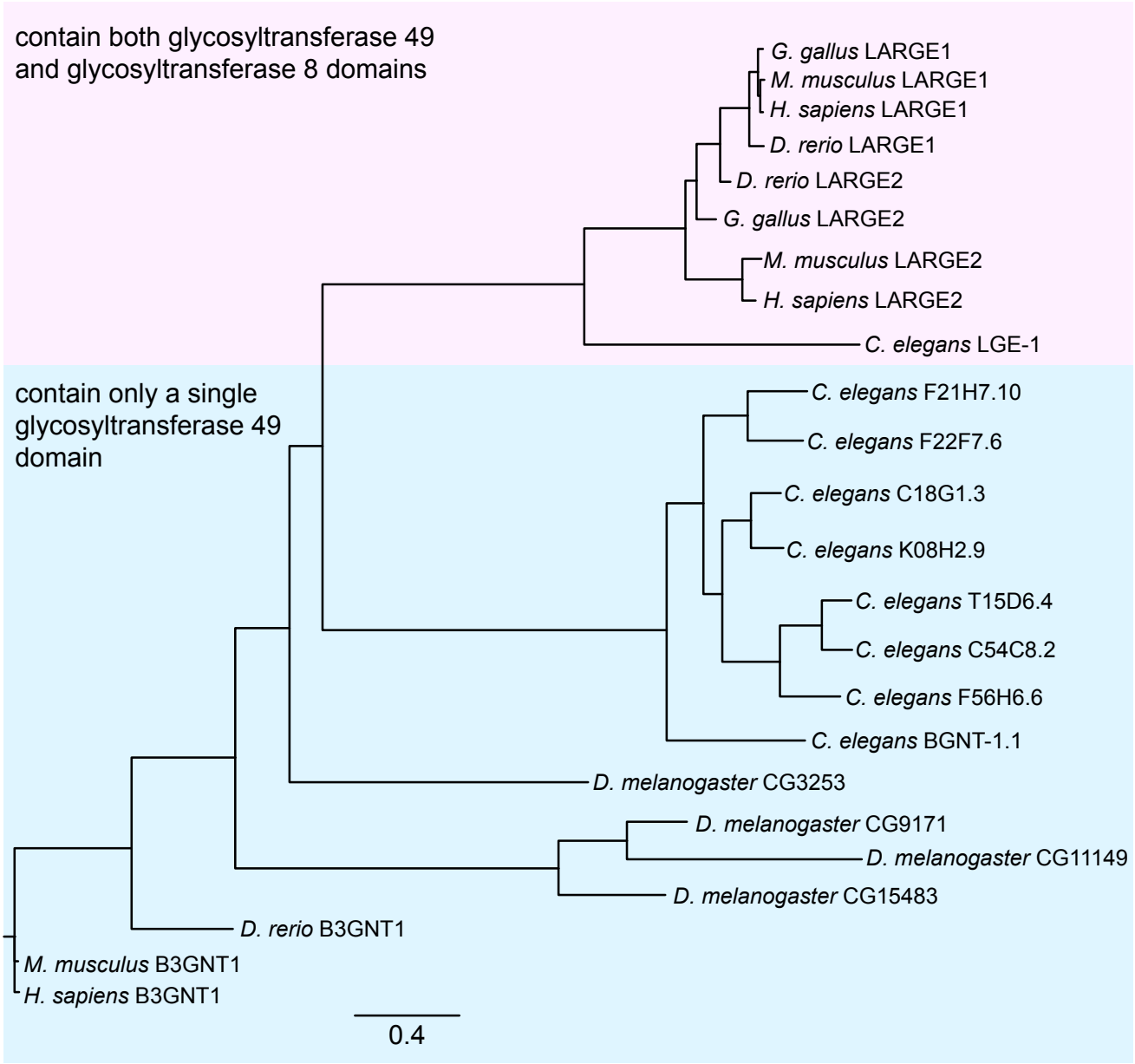

Timbers et al., Figure S4

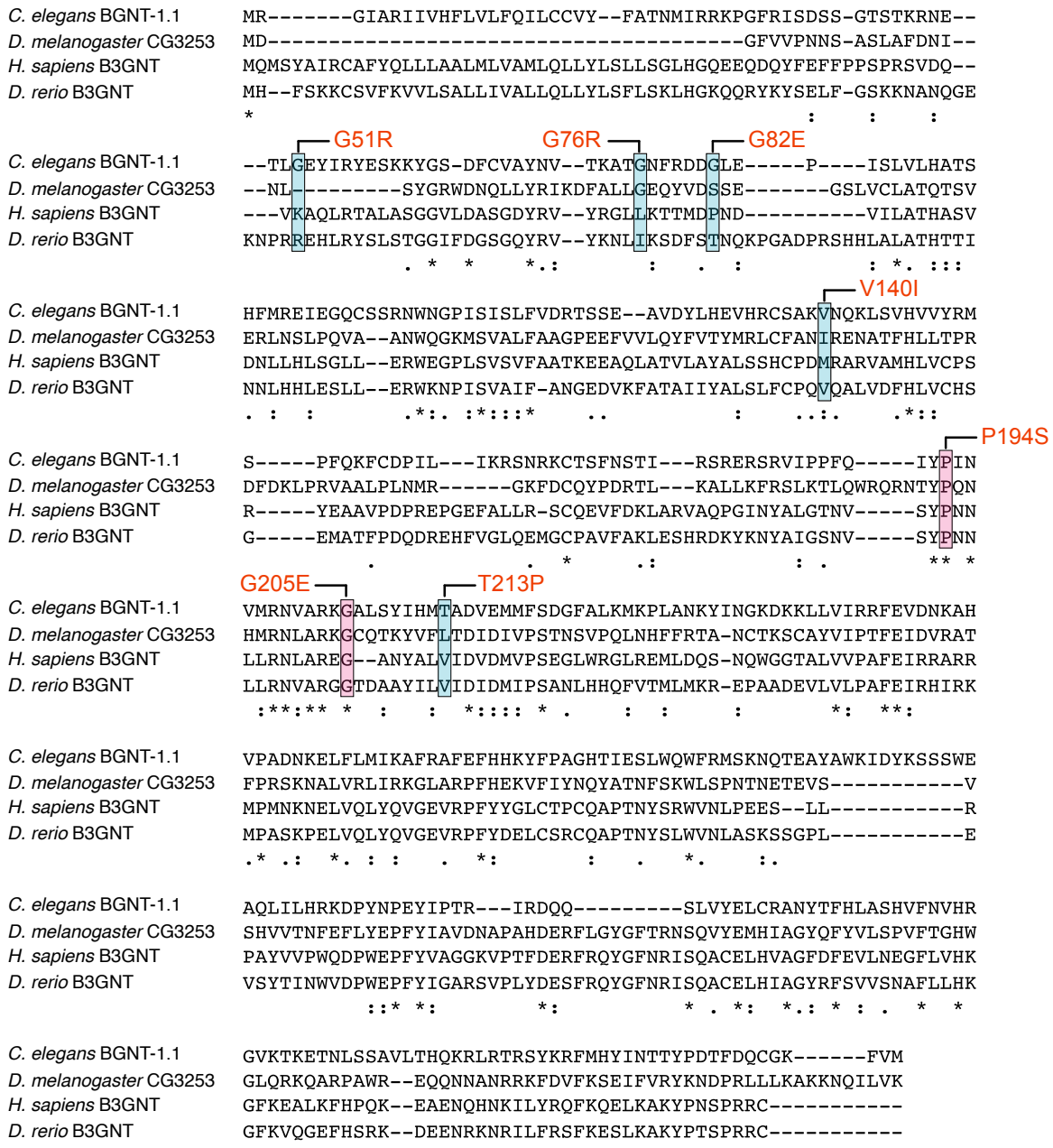

Timbers et al., Figure S5

a Chromosome SNP-mapping of VC20615 *dyf* phenotype

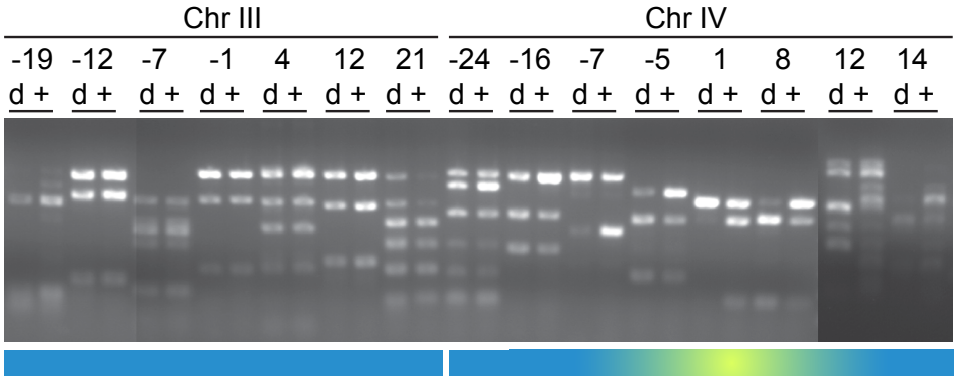

b Chromosome SNP-mapping of VC20628 *dyf* phenotype

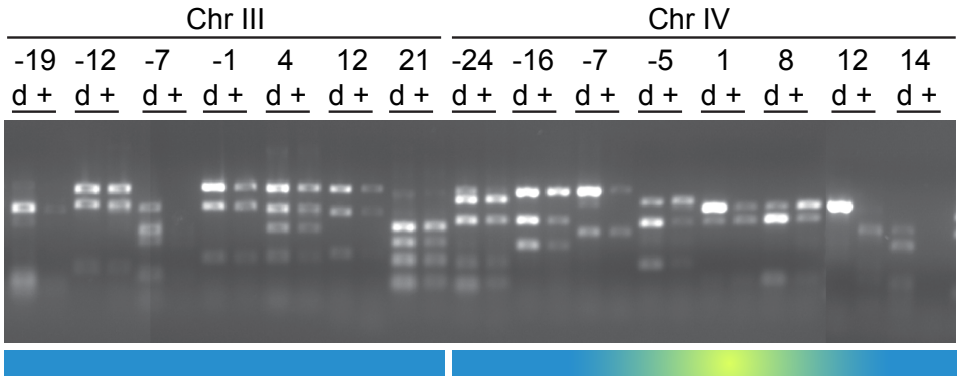

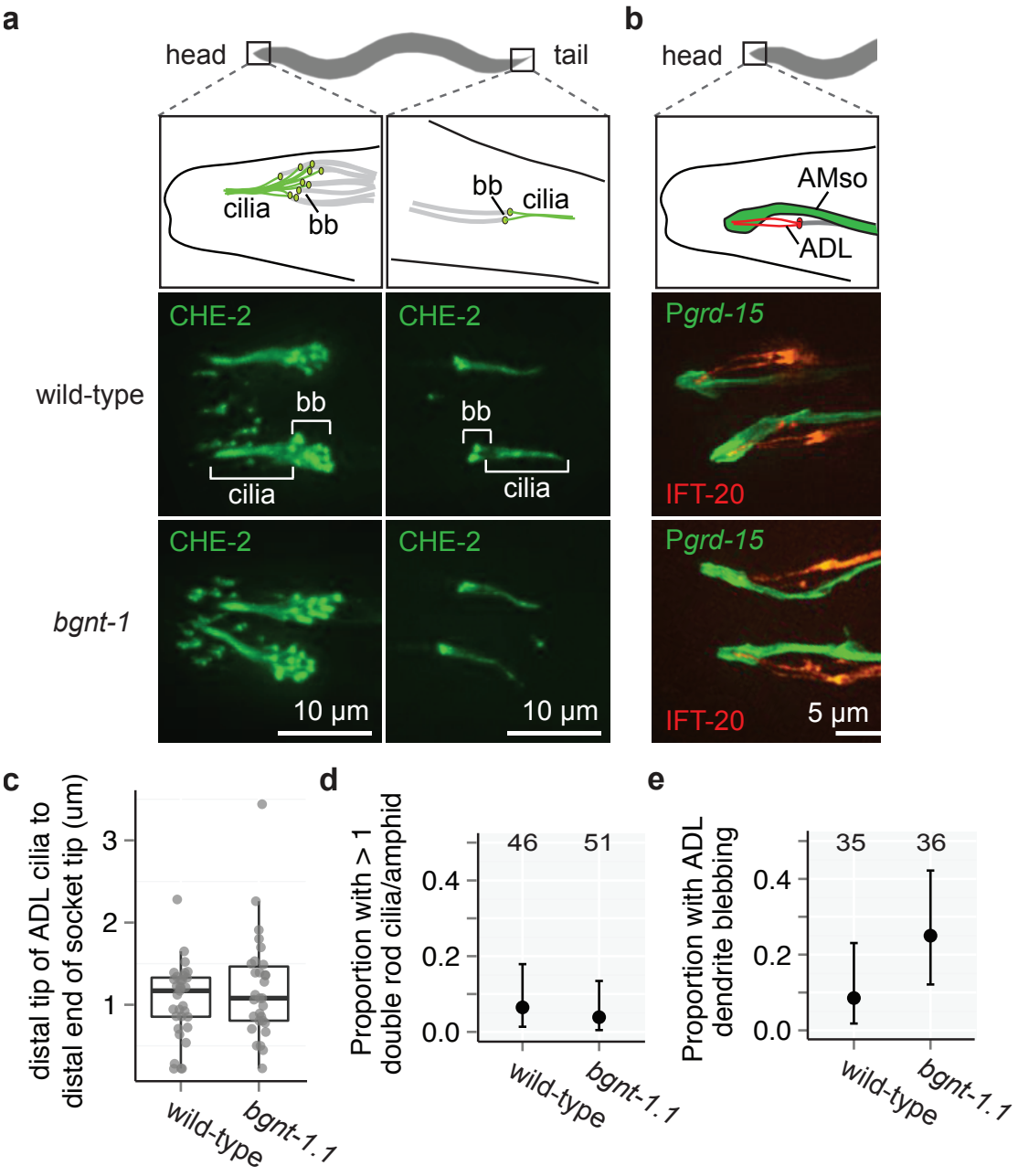

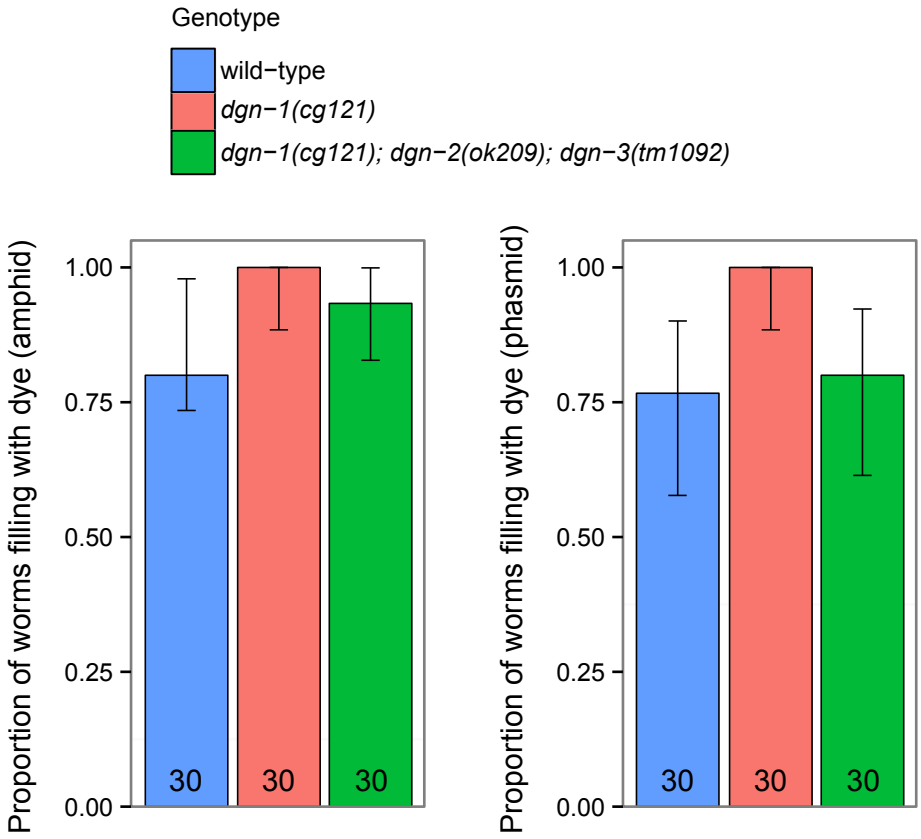

Timbers et al., Figure S8

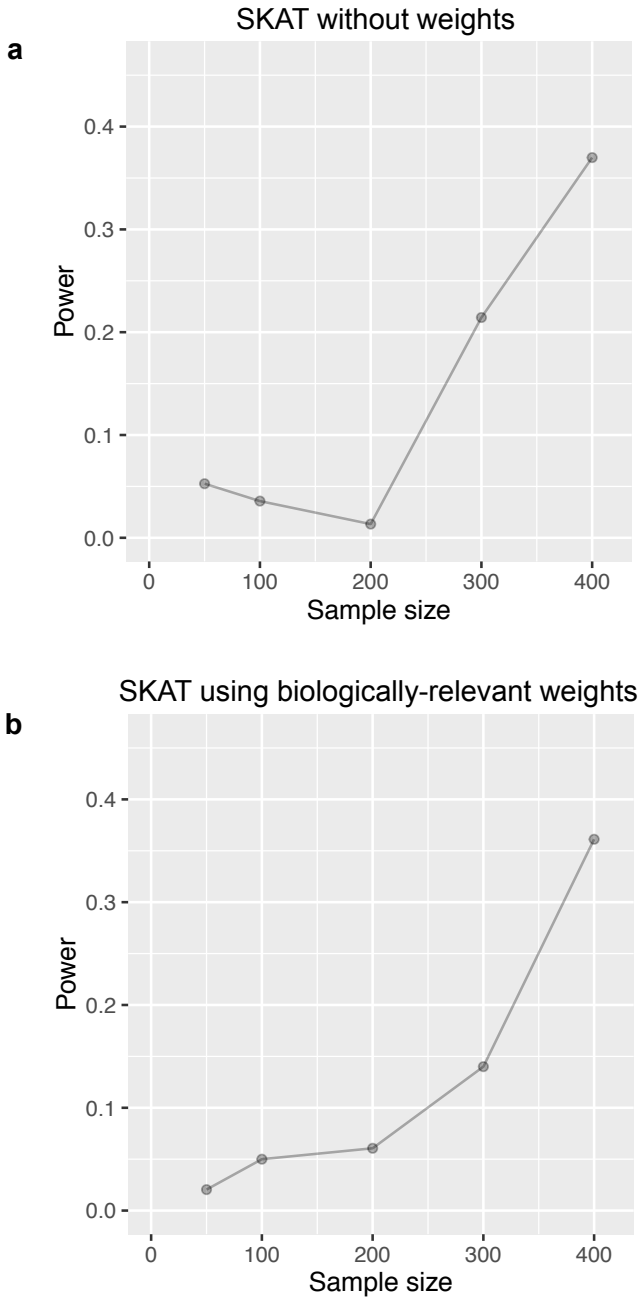

Timbers et al., Figure S9

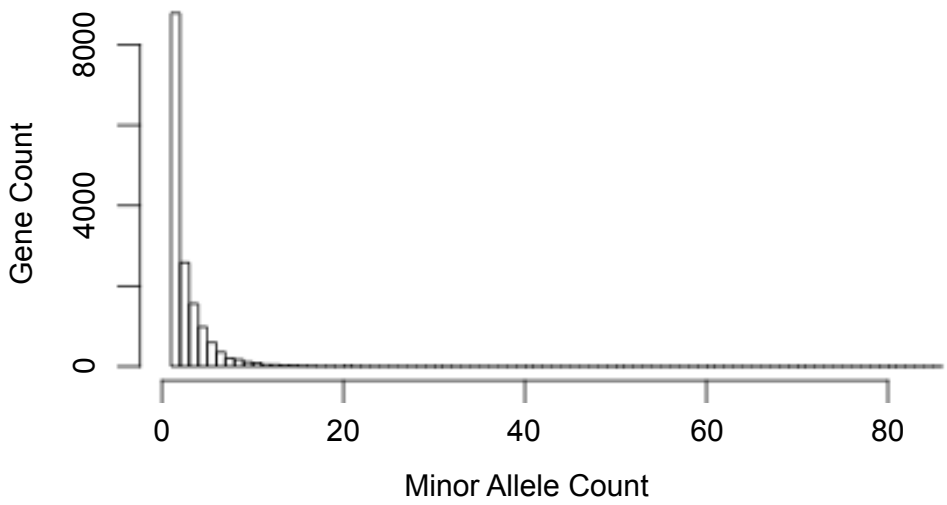

Timbers et al., Figure S10